BIOCHEMISTRY

 Volume 44, Number 14 April 12, 2005

Articles

Inhibitor and Ion Binding Sites on the Gastric H,K-ATPase†

Keith Munson,* Rachel Garcia, and George Sachs

Geffen School of Medicine, University of California at Los Angeles, and VAGLAHS, Los Angeles, California 90073

Received October 20, 2004; Revised Manuscript Received December 15, 2004

ABSTRACT: The gastric H,K-ATPase catalyzes electroneutral exchange of H^+ for K^+ as a function of enzyme phosphorylation and dephosphorylation during transition between E_1/E_1-P (ion site in) and E_2-P/E_2 (ion site out) conformations. Here we present homology modeling of the H,K-ATPase in the E_2-P conformation as a means of predicting the interaction of the enzyme with two known classes of specific inhibitors. All known proton pump inhibitors, PPIs, form a disulfide bond with cysteine 813 that is accessible from the luminal surface. This allows allocation of the binding site to a luminal vestibule adjacent to Cys813 enclosed by part of TM4 and the loop between TM5 and TM6. K^+ competitive imidazo-1,2α-pyridines also bind to the luminal surface of the E_2-P conformation, and their binding excludes PPI reaction. This overlap of the binding sites of the two classes of inhibitors combined with the results of site-directed mutagenesis and cysteine cross-linking allowed preliminary assignment of a docking mode for these reversible compounds in a position close to Glu795 that accounts for the detailed structure/activity relationships known for these compounds. The new E_2-P model is able to assign a possible mechanism for acid secretion by this P_2-type ATPase. Several ion binding side chains identified in the sr Ca-ATPase by crystallography are conserved in the Na,K- and H,K-ATPases. Poised in the middle of these, the H,K-ATPase substitutes lysine in place of a serine implicated in K^+ binding in the Na,K-ATPase. Molecular models for hydronium binding to E_1 versus E_2-P predict outward displacement of the hydronium bound between Asp824, Glu820, and Glu795 by the $R-NH_3^+$ of Lys791 during the conformational transition from E_1P and E_2P. The site for luminal K^+ binding at low pH is proposed to be between carbonyl oxygens in the nonhelical part of the fourth membrane span and carboxyl oxygens of Glu795 and Glu820. This site of K^+ binding is predicted to destabilize hydrogen bonds between these carboxylates and the $-NH_3^+$ group of Lys791, allowing the Lys791 side chain to return to its E_1 position.

The gastric H,K-ATPase is a member of the P_2-type ATPase family and undergoes a cycle of phosphorylation and dephosphorylation coupled to the outward and inward transport of hydrogen and potassium ions, respectively, in the secretory canaliculus of the parietal cell. Conformations of the enzyme that bind ions for outward transport are defined as E_1, whereas those that bind luminal ions for inward transport are termed E_2. Ion binding to E_1 activates phosphorylation from MgATP to form the intermediate E_1-P, which then converts to E_2-P in the acid transporting step. In the gastric H,K-ATPase as well as the Na,K-ATPases, K^+ binding to E_2-P stimulates dephosphorylation to give the occluded form $E_2{\cdot}K^+_{occ}$ followed by conversion to $E_1{\cdot}K^+$ and release of K^+ to the cytoplasm.

† This work was supported in part by NIH Grants R01 DK-53642, 46917, 58333, and 41301 and USVA Merit Award 0013.

* Address correspondence to this author at VAGLAHS/West LA, Building 113, Room 324, 11301 Wilshire Blvd., Los Angeles, CA 90073. Phone: 310-268-4672. Fax: 310-312-9478. E-mail: kmunson@ucla.edu.

10.1021/bi047761p CCC: $30.25
Published on Web 03/15/2005

The gastric H,K-ATPase sustains a 10-fold inward potassium gradient (150 K^+ in, 15 mM K^+ out) and a transmembrane outward hydrogen ion gradient of greater than 1 million fold to generate a luminal pH of 0.8. This is the largest ion gradient generated by a P_2-type ATPase. The exported ions are presumed to be hydronium rather than protons partly because of the ability of Na^+ to act as a competent surrogate for H^+ at pH 8 (*1*). Hence there is functional similarity to the Na,K-ATPase at this pH. The homology in the ion binding residues and the large number of ligands needed to complex three Na^+ ions make it more likely that hydronium is bound than individual protons.

The primary structure of the gastric H,K-ATPase (HK α_1) shows significant homology to the Na,K-ATPase (62%) and the sr Ca-ATPase[1] (29%). The ion binding sites of the H,K-ATPase are homologous to these, and other, P_2-type ATPases in that they have only carboxylate side chains as the counter charge species. This indicates generation of an exceptionally low pK_a for one of these carboxylate enclosed sites in the H,K-ATPase. In vitro vesicle transport measurements carried out at pH 6.1 to avoid proton release from the hydrolysis of ATP have shown that two H^+ and two K^+ are transported per ATP hydrolyzed whereas at full acid gradient in vivo (ΔpH $\sim$6.0) only one H^+ can be transported, based on the free energy available from ATP hydrolysis (*2*). Hence one ion binding site must have a low pK_a for transport at pH $\sim$1.0, while a second site with a higher pK_a retains hydronium at highly acidic external pH to give this variable stoichiometry. Another unique feature of this enzyme is the multiplicity of luminally acting inhibitors of the gastric H,K-ATPase. Understanding the mechanism of these drugs is of interest because complete and rapid suppression of acid secretion is a major goal for improving the currently available treatment of acid-related disease.

Two classes of drugs have been developed that both bind only to the outside face of the enzyme in E_2. One class, the proton pump inhibitors (PPIs), is currently in use worldwide. These substituted pyridylmethylsulfinylbenzimidazoles, such as lansoprazole, omeprazole, and pantoprazole, are prodrugs which accumulate in the acidic space of the secretory canaliculus and then are acid-activated to form cationic, thiophilic intermediates. These react with one or more cysteine sulfhydryls at the luminal surface of the pump to form disulfide bonds. It is known that all PPIs bind to cysteine 813 (*3*), resulting in covalent inhibition of the enzyme via formation of this disulfide which stabilizes the enzyme in the E_2 conformation.

The acid pump antagonists, APAs such as SCH28080, represent a second class of inhibitor now under development. These are reversible, K^+ competitive inhibitors with a substituted 1,2-α-imidazopyridine core structure (*4*, *5*) that also bind to the E_2 form of the ATPase (*6*). Numerous derivatives of APAs have been synthesized and their relative affinities to the pump determined. A model for the molecular structure of inhibitor binding must account for these structure−activity relationships. Further, inhibition by the PPIs and the imidazopyridines is mutually exclusive (*7*), implying that their binding sites overlap and the model must explain this finding. X-ray crystallography of the H,K-ATPase with the inhibitor bound would provide the desired structures and aid in the design of improved versions of these inhibitors, but it has not yet been possible to crystallize any of the P_2-type ATPases except the sr Ca-ATPase.

Pioneering X-ray crystallography of the sr Ca-ATPase has provided the first molecular structures of intermediates (or their homologues) formed during ion transport by this P_2-type ATPase. These include E_1 in which two calcium ions are bound, $E_1[2Ca^{2+}]$, E_1 with AMPPCP bound, E_1-[AMPPCP], and E_2 with the specific inhibitor thapsigargin bound, E_2[TG] (*8*−*10*). Recently, a structure was reported for an E_2-P homologue containing thapisgargin, MgADP, and MgF_4^{2-} at the active site as a stable phosphate substitute (*11*). These studies provide an essential framework for understanding the structural basis of P_2-type ATPase ion pumping (*12*).

The sr Ca-ATPase structures show luminal, membrane, and cytoplasmic domains. The cytoplasmic domain has a stalk-like extension rising from the membrane domain closely surmounted by the phosphorylation domain (P domain), a globular nucleotide binding domain (N domain) connected to the P domain by a flexible hinge, and an "actuator" domain (A domain) which assumes various positions around the P domain in the different conformations. The actuator and nucleotide binding domains are widely separated atop the P domain in the $E_1[2Ca^{2+}]$ conformation and are drawn together over the phosphorylation site in E_2[TG] and E_2-P. In the E_1[AMPPCP] form, the N domain is tilted and the adenine binding pocket is oriented to allow proximity of the terminal phosphate of ATP to the phosphorylating site in the P domain. These major reorientations of the cytoplasmic subdomains are associated with significant changes in the relative positions of the TM1 through TM6 helices. These in turn affect the geometry of both ion and inhibitor binding sites (*13*−*15*) and are presumably related to ion transport through the membrane domain.

The availability of the sr Ca-ATPase structures has provided functional interpretations for an array of previously recognized homologous sequence motifs as well as a large number of mutational effects reported for many P_2-type ATPases (*16*, *17*). For instance, the identification of Ca^{2+} ligands in the $E_1[2Ca^{2+}]$ structure and mutation of residues aligned to them in the Na,K- and H,K-ATPases imply a conserved ion binding function for homologous carboxylic acid residues in the fourth, fifth, and sixth transmembrane segments of these pumps. On the other hand, residue differences near otherwise homologous regions represent possible determinants of ion transport diversity. In the gastric H,K-ATPase, a lysine residue (Lys791) in the ion binding site replaces a serine in the Na,K-ATPase implicated in ion transport in this pump (*18*−*20*). The gastric pump K791S mutant is nearly inactive (*21*) and shows a 20-fold lower sensitivity to the specific imidazopyridine inhibitor, SCH28080. This lysine therefore contributes to the 1000-fold greater

[1] Abbreviations: sr Ca-ATPase, sarcoplasmic reticulum Ca^{2+}-ATPase; omeprazole, 5-methoxy-2-[[(4-methoxy-3,5-dimethyl-2-pyridinyl)methyl]sulfinyl]-1*H*-benzimidazole; protein-bound form of pantoprazole, [1-(5-difluoromethoxy-1*H*-benzimidazol-2-yl)-3,4-dimethoxypridinium-2-yl]methyldisulfidyl protein; SCH28080, 3-(cyanomethyl)-2-methyl-8-(phenylmethoxy)imidazo[1,2α]pyridine; Byk99, (7*R*,8*R*,9*R*)-7,8-dihydroxy-2,3-dimethyl-9-phenyl-7,8,9,10-tetrahydroimidazo[1,2-*h*][1,7]naphthyridine; Byk73, (7*R*,8*R*,9*R*)-7,8-dihydroxy-2,3-dimethyl-9-phenyl-10-methyl-7,8,9-trihydroimidazo[1,2-*h*][1,7]-naphthyridine; AMPPCP, adenosine 5′-[β,γ-methylene]triphosphate; RMS, root mean square; PCR, polymerase chain reaction.

sensitivity of the gastric pump to this inhibitor compared to the Na,K-ATPase, and the charged amino group is a candidate for insertion into a carboxylic acid cluster to displace hydronium outward at the low affinity required in E_2-P.

Recent mutational studies of the H,K-ATPase have focused on the ion binding and specific inhibitor sites (*21*−*25*). The effects of residue substitutions on the enzyme activity, $K_{m,app}$ for NH_4^+, and the K_i for SCH28080 have identified key residues in both sites. Most of the mutations that affect inhibitor affinity are clustered in the TM5/TM6 exoplasmic loop, and many mutations can affect inhibitor affinity without affecting ion affinity, showing that the competitive nature of inhibition is due to mutual exclusion and not to direct overlap of inhibitor and ion binding sites (*26*). Of particular interest is a series of mutations that change the nature of the inhibition to mixed or even noncompetitive, suggesting that space is made available for either K^+ or the imidazopyridine to bind simultaneously in contrast to the wild-type enzyme where binding is exclusive (*21*, *23*).

An essential tool for interpretation of biochemical and mutational data and for structure-based inhibitor design is an accurate molecular structure of the target protein. In the present study, we report continuing progress in utilizing molecular modeling and mutagenesis to delineate inhibitor and ion binding sites in this enzyme. The binding region of the imidazopyridine class of inhibitors was mapped in greater detail by expressing and analyzing activity of a large number of membrane domain mutants. It was found that a portion of TM4 adjacent to the TM5/TM6 loop forms an essential part of the site. A new molecular model of the H,K-ATPase in the E_2-P conformation was constructed, and an inhibitor (Byk99) of the imidazopyridine class with high affinity, known stereochemistry, and few free rotamer angles was docked within a region surrounded by side chains shown to be important for binding. The homology modeling utilized the E_2[TG] form of the sr Ca-ATPase as a starting point, followed by replacement of the N domain with the crystal structure of the N domain of the Na,K-ATPase α2 isoform (*27*) and then loop reconstruction and substitution with the H,K-ATPase side chains. The E_2-P conformation was simulated by adding magnesium phosphate to the active site and applying restraints during energy minimization to mimic the phosphorylated form of phosphoserine phosphatase, an enzyme with homologous active site structure (*28*).

The derived structure defines the region of overlap between binding of the covalent proton pump inhibitors and the reversible imidazopyridines and also identifies critical structural regions of the binding sites of the reversible inhibitors. The proposed fit of the inhibitors to the site is consistent with the structure−activity relationships that have been identified for those inhibitors.

The E_2-P model described here further explains the ability of the H,K-ATPase to expel a proton or hydronium from a cluster of carboxylic side chains at an external pH of 0.8 in exchange for a single K^+ while, on the other hand, transporting two H^+ and two K^+ per ATP at less acidic luminal pH. In the cytoplasmic domain the model is consistent with the observed sites of Fe^{2+}-catalyzed backbone cleavage in the vicinity of the active site (*29*, *30*). This model will provide a framework for future structural investigations of the gastric H,K-ATPase.

EXPERIMENTAL PROCEDURES

Homology Modeling and Energy Minimization. A combination of methods was used to model the H,K-ATPase in the E_2-P conformation, the state that releases hydronium with a low pK_a and binds luminal K^+ at pH ∼1.0. The starting point for the model was the sr Ca-ATPase E_2[TG] backbone (structure file pdb.1iwo). This structure was modified by replacing the N domain with that of the Na,K-ATPase α2 N domain solved by crystallography (pdb.1q3i). In contrast to the sr Ca-ATPase, the H,K-ATPase sequence is unambiguously aligned with the Na,K-ATPase in this domain (see Appendix, Figure 7). To generate the phosphorylated state, Mg^{2+} and acyl phosphate at Asp385 were added to the active site in positions analogous to those found in phosphoserine phosphatase, an enzyme with a homologous active site fold (*28*). Pantoprazole, a PPI known to modify both Cys813 and Cys822 by disulfide linkage, was added at these positions as a final structural constraint (*31*). Distance restraints were applied within the active site as defined in phosphoserine phosphatase, and a combination of energy minimization and molecular dynamics with distance restraints between hydrogen bond donors and acceptors in all helices gave the E_2-P model with two pantoprazoles bound. Subsequently, an energy-minimized E_2-P model for reversible inhibitor binding was constructed after deleting both pantoprazole moieties and docking the high-affinity imidazopyridine, Byk99, in the site defined by mutagenesis. This model was then used to energy minimize distinct ion-bound states of the transport site with Byk99 removed. These variants changed very little in the RMS deviation of backbone atoms (<∼0.5 Å). The sequence alignments and detailed modeling methods are given in the Appendix.

H,K-ATPase Mutation and Expression. These procedures have been described in detail previously (*21*−*23*). Briefly, plasmid, pcDNA3.1(Zeo), containing the wild-type rabbit gastric H,K-ATPase α subunit sequence was used as a template to generate single mutants by using appropriate primers and the QuikChange PCR kit (Stratagene). After transformation and colony selection, plasmids (0.1−0.2 mg) were prepared (Qiagen midi kit) and sequenced to verify the presence of the desired mutation. When double mutants were desired, the process was repeated using plasmids of the single mutants for templates. Transfections were performed by using the calcium phosphate method in a HEK293 cell line stably expressing a high level of the H,K-ATPase β subunit. Selection with zeocin generated colonies which were screened via Western blots (antibody 12.18) to identify the highest expressing clones. These were grown en masse and homogenized, and a light membrane fraction was isolated on top of 40% sucrose in 10 mM Pipes/Tris, pH 7, 2 mM EGTA/Tris, and 2 mM EDTA/Tris, then washed in buffer without sucrose, resuspended by homogenization, and stored at −80 °C. In some experiments an entire plate of selected colonies was expanded and used for membrane isolation, and these are designated in Table 1 as "multiclone". The amount of expressed H,K-ATPase per milligram of membrane protein (Lowry) was determined by quantitative Western blot analyses using purified pig gastric H,K-ATPase membranes as a standard. This preparation ("G1" membranes) has a purity corresponding to a content of 85% α and β subunits and provides the basis for normalization of the mutant

Table 1: Effect of Side Chain Mutation in the Membrane Domain on the H,K-ATPase

location	mutant	K_i[SCH] (nM)	type of inhibition	V_{max} (μmol mg^{-1} h^{-1})	$K_{m,app}$[NH_4^+] (mM ± SE)
	(A) Mutations Significantly Affecting K_i for SCH28080				
	wt[a]	64 ± 11	comp	132 ± 3	2.4 ± 0.1
TM4	R328E/Y324C	493	mixed	22	0.7 ± 0.3
	M330V	212	comp	30	3.3 ± 0.7
	F332I	4000	mixed	14	4.5 ± 1.4
	M334A	450	comp	29	0.8 ± 0.2
	M334I (clone 15)	960	comp	30	4.6 ± 1.3
	M334I (clone 7)	840	comp	29	3.2 ± 1.4
	M334C	520	comp	60	2.2 ± 0.3
	A335S	1200	comp	30	3.5 ± 0.4
	A335C		none	67	2.5 ± 0.3
	A335C/C813A	40000	comp	69	3.8 ± 0.3
	V338I	400	mixed	14	2.2 ± 0.3
	A339S	220	mixed	27	3.5 ± 1.0
	L809C/F332C	270	mixed	40	3.5 ± 0.4
TM5	E795D[b]	700	comp	10	8.1 ± 2.6
	K791S[b]	1325	comp	7	4.7 ± 0.3
TM5/TM6 loop	L809F[c]	6150	noncomp	89	1.9 ± 0.3
	P810G[c]	563	comp	109	2.4 ± 0.2
	L811F[c]	625	mixed	113	2.0 ± 0.1
TM6	C813T[c]	586	comp	40	6.6 ± 1.8
	I816L[c]	309	noncomp	31	1.4 ± 0.4
TM8	T929L[c]	512	comp	27	1.2 ± 0.2
	(B) Mutations with No Significant Effect on Inhibitor Affinity				
TM3	F315Y	50	mixed	44	1.2 ± 0.07
TM4	G323E	77	comp	232	2.0 ± 0.1
	F326W	70	comp	194	2.0 ± 0.1
	V331I (multiclone)	76	mixed	37	2.6 ± 0.7
	V331F	48	mixed	68	1.0 ± 0.08
	F333A (multiclone)	56	mixed	29	3.4 ± 0.6
	F333L	160	comp	58	3.7 ± 0.5
	A335G	16	comp	31	3.4 ± 0.3
	I336L	92	comp	41	0.7 ± 0.1
	V337I (multiclone)	97	comp	95	0.7 ± 0.3
	V337I (clone 5)	108	comp	64	0.8 ± 0.1
	A339C	180	mixed	44	0.9 ± 0.1
	Y340N	140	comp	1.5	1.6 ± 1.0
TM5/TM6	L809C	62	mixed	83	4.2 ± 0.3

[a] Standard errors for the V_{max} and K_i calculated from assay data were proportional to those given for the $K_{m,app}$. V_{max} was normalized to protein expression. Improved analyses altered previously reported values for V337I and R328E/Y324C (*22*). [b] From ref *21*. [c] From ref *23*.

ATPase activity, making the normalized V_{max}, nanomoles per microgram of expressed H,K-ATPase per hour, equivalent to the specific activity of the mutant.

ATPase Assay. ATPase analyses used 3−10 μg of total membrane protein (~100 ng of expressed H,K-ATPase), 0.8 mM TrisATP containing [^{32}P]ATP (3000 cpm/nmol), Na^+-free reaction buffer [40 mM Tris-HCl (pH 7.4) and 2 mM $MgCl_2$ in a total volume of 150 μL with a range of NH_4Cl concentrations (0−40 mM)], and various SCH28080 concentrations for 60 min at 37 °C. Also included were 1 mM EGTA (Ca-ATPases), 500 μM ouabain (Na,K-ATPase), 1 μM oligomycin (mitochondrial ATPase), 10 nM bafilomycin (V-type ATPases), and 100 nM thapsigargin (sr Ca-ATPase) to suppress the activities of possible contaminating ATPases in the membrane fraction. Reactions were terminated with 150 μL of 4.5% ammonium molybdate in 14% perchloric acid and extracted with 0.4 mL of butyl acetate at 4 °C. After brief centrifugation (1 min) at low speed (500 rpm) 200 μL of the butyl acetate layer was counted. In each data set the background ATPase in the absence of ammonium was subtracted from the ion-stimulated activity. Kinetic parameters V_{max} (in micromoles per milligram of expressed H,K-ATPase per hour), $K_{m,app}$ (apparent ammonium affinity), and K_i (SCH28080 affinity) were determined by fit of the data to the Michaelis−Menten equation. The standard error within individual sets of ATPase assays was dependent on the level of ammonium-stimulated activity which increased with expression level and mutant specific activity and ranged from 10% to 100% above the zero-ion background.

RESULTS AND DISCUSSION

The results will be presented first as a general description of the homology model with emphasis on the membrane domain and the binding sites for pantoprazole. Key distances between TM4 and TM6 across one of the pantoprazole sites in the model are then confirmed by cysteine replacements and cross-linking. A detailed description of the reversible inhibitor binding site is presented that is based on the results of site-directed mutagenesis and the overlap with the binding site of pantoprazole at cysteine 813. Finally, hypotheses are presented for both outward hydronium and inward K transport on the basis of the model.

Modeling the Gastric H,K-ATPase α *Subunit in the E_2-P Conformation.* A combination of approaches was used to define PPI and APA binding sites on the H,K-ATPase. First we used detailed homology modeling to the known E_2[TG] form of the sr Ca-ATPase, pdb.1iwo, with substitution of

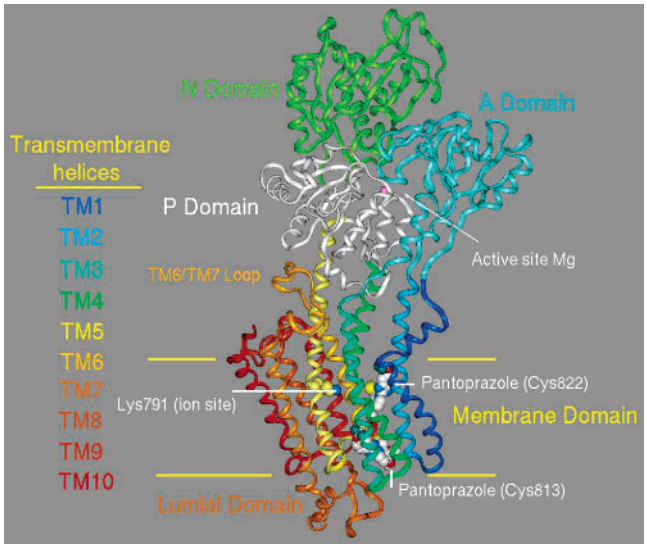

FIGURE 1: Homology model of the gastric H,K-ATPase α subunit in the E_2-P conformation. The model is oriented vertically with respect to the plane of the membrane (yellow lines) and illustrates the juxtaposition of nucleotide binding (N), actuator (A), and phosphorylation (P) domains in the E_2-P conformation. Transmembrane (TM) segments encompassing the membrane, stalk, and luminal domains are color coded from the N- to C-terminus (color scheme is maintained in all figures; TM1, dark blue; TM2, cyan; TM3, light green; TM4, green-blue; TM5, light yellow; TM6, dark yellow; TM7, light brown; TM8, dark brown; TM9, light red; TM10, dark red). The position of the ion binding site is close to K791 (ball and stick representation). The proton pump inhibitor, pantoprazole (CPK), forms disulfide bonds (yellow spheres) at Cys813 and Cys822. The active site Mg^{2+} is illustrated with a pink sphere in the P domain.

the more homologous N domain from the Na,K-ATPase α2 isoform. Structures for two pantoprazole moieties were added to their biochemically defined sites of cysteine modification, Cys813 and Cys822, to act as structural constraints (Figure 1). Molecular dynamics and energy minimization with restraints to mimic key interactions in the active site deduced from phosphoserine phosphatase were used to simulate the E_2-P conformation with the two inhibitor moieties bound. Internal cysteine cross-linking in site-directed mutants was used to verify key helix orientations in the model next to Cys813. A series of mutants in the region of Cys813 were expressed and tested for their ability to bind the reversible K^+ competitive imidazopyridine, SCH28080. Finally, the pantoprazole groups of the initial model were deleted, and the high-affinity imidazopyridine, Byk99, was docked with energy minimization in a site adjacent to Cys813 which was defined by the mutagenesis results. The model is presented first in terms of the general arrangement of the E_2-P conformation followed by discussion of the membrane domain as the major focus of this report. The conformation of the cytoplasmic domain is discussed in the Appendix.

General Arrangement of the Model. The E_2-P model of the H,K-ATPase (Figure 1) may be divided into domains equivalent to those defined for the sr Ca-ATPase (*8*). These include a cytoplasmic domain comprised of nucleotide binding (N, green), actuator (A, light blue), and phosphorylation (P, white) subdomains, a membrane domain, and a small luminal domain. The model is oriented approximately perpendicular to the plane of the membrane (*9*), showing the tilts of the transmembrane helices (color coded in Figure 1 and boxed in the sequence alignment) and approximate position of the ion binding site within the bilayer. Membrane helices with major extensions into the stalk include TM2, TM3, TM4, and TM5. The TM1 helix is bent near the membrane surface, dividing it into membrane and cytoplasmic sections. The membrane boundaries (yellow lines) are estimated from the positions of hydrophilic side chains at either end of the hydrophobic helix segments. The backbone closely superimposes homologous positions in pdb.1iwo with a backbone RMS of 2.83 Å, calculated from the bolded sequences in Figure 7 of the Appendix. The model shows changes in the relative positions of the cytoplasmic subdomains which are more closely arranged around the magnesium ion at the active site than in the E_2[TG] form of the sr Ca-ATPase. In this respect the H,K-ATPase model more closely resembles the E_2-P conformation of the sr Ca-ATPase (pdb.1wpg) even though the overall overlap (RMS of 3.9 Å) is more divergent because in the sr Ca-ATPase there is a slightly greater tilt in the P, N, and A domains as a group with respect to the plane of the membrane and because of a small rotation of the N domain altering its interface with A. The N domain in the sr Ca-ATPase E_2-P homologue also contains bound MgADP at its interface with A that is not included in the H,K-ATPase model.

Membrane Domain. The membrane domains of the H,K-ATPase E_2-P model and the sr Ca-ATPase in E_2[TG] are distinct in several ways. Backbone modeling required deletions in the TM3/TM4 loop which truncated the TM4 helix at its luminal end and insertions in the TM1/TM2 loop resulting in extension of the TM2 helix (see alignment in Figure 7 of the Appendix). These changes occur in the vicinity of the K^+ competitive inhibitor binding domain as described in detail below. Backbone insertions also were necessary before TM7 and in the TM7/TM8 luminal and TM8/TM9 cytoplasmic loops. The structure derived for the TM7/TM8 loop contains a short exposed region, S[910]YGQ, known to interact with the β subunit (Figure 2). The TM8/TM9 loop was modeled to follow the plane of the apparent membrane surface as in the sr Ca-ATPase structure. It has been proposed the TM7/TM10 microdomain acts as a membrane anchor based on the small changes in its position during the E_1/E_2 transition. Interaction of the TM8/TM9 loop at the membrane surface would support this role (*12*).

It is of interest to compare the positions of the transmembrane helices in the present model to those in the E_2[TG] (pdb.1iwo), E_1-P (pdb.1wpe), and E_2-P (pdb.1wpg) conformations of the sr Ca-ATPase. This is best accomplished by superimposing transmembrane segments TM5 to TM10. For example, the overall RMS deviation in the backbone positions of E_2[TG] compared to E_2-P is 4.34 Å whereas the deviation is only 1.39 Å in the backbone atoms from TM5 to TM10 and only 2.45 Å deviation over the same region of E_1-P. Hence the conformation of TM5 through TM10 changes comparatively little during catalysis although some of these changes are critical (e.g., in TM5 through TM6). Comparison of the superimposed E_2[TG] and E_2-P forms of the sr Ca-ATPase reveals a subtle increase in the separation of the TM1 to TM4 helices in the latter (especially the luminal half of TM4), and this may be revealing a path for ion exit/entry from the lumen between these segments and TM5/TM6. As expected, the H,K-ATPase model from TM5 to TM10 superimposes closely onto the E_2-P homologue of

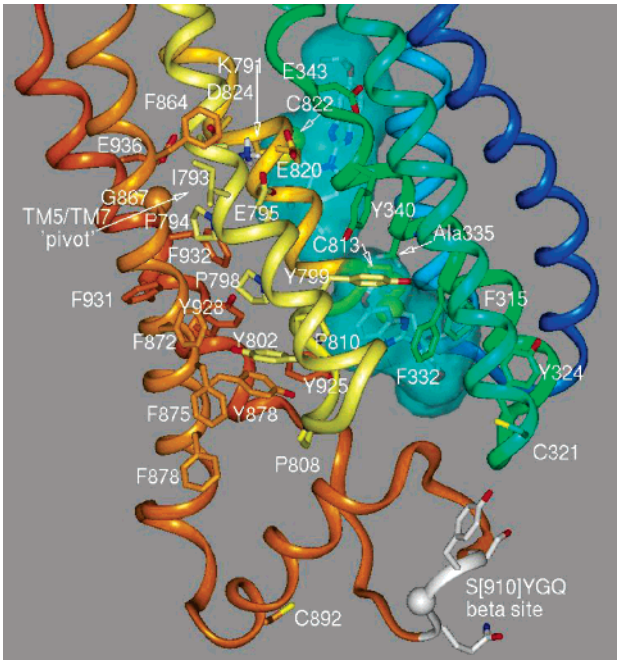

FIGURE 2: Membrane domain of the H,K-ATPase E_2-P model with pantoprazole, bound at Cys813 and Cys822 (stick with Connolly surfaces in cloud). A known site of β subunit interaction (*36*, *37*), S[910]YGQ, is highlighted (white ribbon) in the TM7/TM8 loop. Cys813, Cys892, and Cys321 are labeled (*38*) by various proton pump inhibitors (all at Cys813, omeprazole at Cys892, and lansoprazole at Cys321) and are solvent-accessible in the model. Labeling at the latter two sites is not correlated with inhibition (*3*). The crossover point ("pivot") between TM5 near Ile793 and TM7 near Gly867 (gold sphere) is apparently conserved in the P_2-type ATPases. An extensive array of aromatic side chains (in stick form) replaces nonaromatic sr Ca-ATPase residues and affects the spacing between helices. TM9 and TM10 are omitted for clarity.

the sr Ca-ATPase (RMS deviation 4.05 Å). The separation of the TM1 to TM4 helices from the TM5/TM6 loop is greater, however, in the H,K-ATPase model with TM1, TM3, and TM4 especially displaced and more tilted with respect to the membrane plane than their sr Ca-ATPase counterparts. This is a result of the presence of the bound inhibitor in the space between these segments in the modeled H,K-ATPase. Hence the model supports and expands the predicted ion entry path. The mechanism of the K^+ competitive imidazopyridine class of inhibitor is believed to be obstruction of ion access to the ion transport site. The larger separation of the membrane helices required for inhibitor docking suggests greater dynamic motion in this part of the membrane domain than revealed in the sr Ca-ATPase models.

The TM1 and TM2 helices in the membrane domain of the sr Ca-ATPase show large changes in position during the E_1/E_2 transition. These in turn are associated with different positions of the actuator domain to which they are directly linked. Particularly significant is a bend in the TM1 helix seen in E_2 but not E_1. Similar structural changes are presumed to be part of the mechanism in all P_2-type ATPases. This is supported by the amphipathic nature of the cytoplasmic portion of the TM1 helix (TM1′) in the H,K-ATPase E_2-P model where the surface facing the membrane is hydrophobic and that facing the cytoplasm is hydrophilic. The same feature is found in TM1′ of the sr Ca-ATPase, and this may help to stabilize the bent conformation in E_2. There is, however, a lack of strict sequence homology in the TM1/TM2 region although the sequence similarity in the hydrophobic segments is high and the sequence QE is conserved at the end of TM2. Further evidence for the accuracy of the alignment (Figure 7, Appendix) in TM1 comes from considering the apparent function of the H,K-ATPase sequence L[105]AGGL matched to F[57]EDLL of the sr Ca-ATPase. The latter sequence undergoes the helix−coil transition in the bent portion of TM1 in the sr Ca-ATPase. The GG sequence is conserved in all H,K- and Na,K-ATPases, and the absence of side chains would appear to provide a natural flex point in the TM1 helix.

The orientation of TM7 in the present structure is different from that proposed earlier for the H,K-ATPase (*21*). The gaps inserted into the sr Ca-ATPase sequence at the beginning of TM7 were not included in previous alignments, and they affect the positions on the sr Ca-ATPase backbone used to map the H,K-ATPase side chains in TM7. In the absence of this adjustment, Arg852 in -RLVNE- maps to a buried position on the sr Ca-ATPase backbone, which is inconsistent with its rapid and specific trypsinolysis in the native H,K-ATPase (*3*, *32*). The two extra residues in the H,K-ATPase corresponding to the gaps in the sequence alignment with the sr Ca-ATPase allowed a small loop to be constructed at the entrance to TM7 with Arg852 exposed (see Appendix, Figure 10) and -LV- in buried positions structurally equivalent to -LI- aligned in the sr Ca-ATPase. Moreover, gap insertion allowed alignment of the sequence -IG- in TM7. This sequence is apparently conserved in all H,K- and Na,K-ATPases and has been identified as a "pivot point" between TM5 and TM7 helices in the sr Ca-ATPase (*12*), making its alignment likely based on conserved function (Figure 2). Finally, in the absence of the gaps, three residues which are replaced in the highly homologous amino acid sequence (gb: AAP35241) of the sting ray H,K-ATPase mapped to inward facing positions on the sr Ca-ATPase backbone. This would be opposite to the behavior of all of the other nonhomologous residues in the membrane domain of this evolutionarily distant pump (see Appendix, Figure 8) and contrary to expectations for a homology model where protein/protein contacts are assumed to be conserved.

The H,K-ATPase membrane domain has a large number of aromatic residues as compared to the sr Ca-ATPase (Figure 2). This increases the distance separating TM5 and TM4 between Tyr340 and Tyr799, TM5 and TM8 between Tyr925, Tyr928, and Phe932, and TM5 and TM7 between Tyr802 and Tyr878. Prolines at positions 794 and 798 change the direction of, and partially expand, the TM5 helix just below the ion site. These changes presumably affect the arrangement and specificity of the ion sites and their entry/exit paths as well as the sensitivity to specific inhibitors.

The two known sites of covalent modification by pantoprazole are in the membrane domain (Figure 2). Side chain modification of Cys813 by all of the PPIs is correlated with inhibition (*3*) and requires the existence of a luminal vestibule adjacent to the beginning of TM6. Inhibitor occupancy of the vestibule prevents access to the ion binding site 15 Å away (near Lys791 in the middle of the membrane) and fixes the enzyme in the E_2 configuration. Binding of the PPIs and inhibition at Cys813 are reversed by treatment with thiol reductants, demonstrating solvent accessibility in this position as suggested in the model. Pantoprazole (CPK) is unique among the PPIs in labeling Cys822 in addition to Cys813,

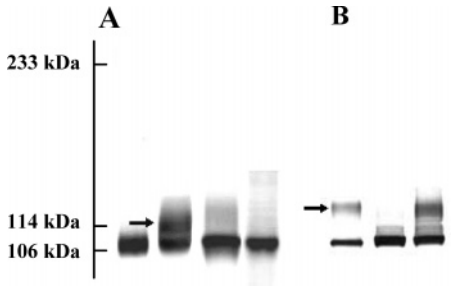

FIGURE 3: Western blot analyses of intramolecular cross-linking in A335C and F332C mutants. (A) Purified gastric H,K-ATPase (G1 std, lane 1, far left) shows the α polypeptide migrating at 106 kDa. Copper phenanthroline cross-linked α−α dimer was observed at 233 kDa in this gel (6% acrylamide). A band representing internally cross-linked α subunit in the A335C mutant (lane 2) migrated at 114 kDa apparent mass (arrow) just above the wild-type α subunit. The band was sensitive to reduction (lane 3) at high concentrations of DTT and β-mercaptoethanol (0.1 and 0.8 M, respectively, pH 8.8, in 1% SDS, 37 °C for 50 min) and was absent in the A335C/C813A double mutant (lane 4). (B) The F332C mutant (lane 2) gave a similar band (lane 3) only upon treatment with $CuCl_2$ (0.15 mM) as shown by comparison to A335C (lane 1) with improved resolution in 8% gels (cross-linked species at the arrow).

and although half of the labeling is released by reduction, inhibition is unaffected, suggesting that the disulfide linkage at Cys822 is solvent-inaccessible and that binding here also fixes the enzyme in the E_2 conformation (*33*, *34*). This known inaccessibility to reducing agents is supported in the model where Cys822 is deep in the membrane at the same depth as ion site residues Thr823 and Asp824 but facing the lipid between now widely spaced TM2 and TM9 helices. In the E_1 conformation Cys822 in TM6 interfaces directly with the TM9 helix, and there is no access of the reactive form of pantoprazole (*33*). Hence disulfide linkage with the bulky inhibitor would prevent the E_2 to E_1 conformational transition of the membrane domain. A similar mechanism has been proposed for steric inhibition of the sr Ca-ATPase by thapsigargin binding between TM3, TM5, and TM7 (*12*) and for phospholamban between TM2, TM6, and TM9, a position analogous to that predicted for pantoprazole at Cys822 (*35*).

Mutations To Define Cys813 Associations Validating Distances Derived from the Model. The predicted orientation of Cys813 and Ala335 across the binding site cleft was demonstrated directly by spontaneous disulfide formation in the A335C mutant which was eliminated in the double mutant A335C/C813A (Figure 3). Not all of the α subunit is cross-linked, indicating the reaction probably occurs only transiently in a specific short-lived membrane compartment during vesicle trafficking. Cross-linking would be expected to produce inactivation as in PPI modification, and the observed activity and SCH28080 resistance must be properties of un-cross-linked enzyme. The internally cross-linked species was observed by SDS−PAGE at 114 kDa, well separated from the α−α dimer produced by copper phenanthroline treatment, and was partially cleaved under strongly reducing conditions (0.1 M DTT and 0.8 M β-mercaptoethanol) but insensitive to mild reduction (20 mM β-mercaptoethanol), suggesting poor accessibility of the reductant to the cross-linked species. The anomalous migration of this species may indicate reduced SDS binding and a lower charge to mass ratio compared to un-cross-linked peptide. Cross-linking between cysteines requires a distance between α carbons between 4 and 7.5 Å (*39*) whereas the distance in the model with Byk99 bound described below is 8.4 Å. Hence, a smaller span in the width of the cleft is possible prior to Byk99 binding. A similar internally cross-linked species is formed in the F332C mutant treated with $CuCl_2$ (0.15 mM). The α carbons of Phe332 and Cys813 are separated by 9.7 Å in the E_2-P model and 5.7 Å in an E_1 homology model for the H,K-ATPase (*21*), suggesting likely disulfide formation in the latter conformation. The cross-linked species in the F332C mutant demonstrated similar chemistry to that of A335C with the same apparent mass and resistance to mild reduction (20 mM β-mercaptoethanol), suggesting likely disulfide formation rather than a Cu^{2+} linkage. The distances derived from this approach are consistent with the distances in the homology models.

H,K-ATPase Inhibitor Binding Sites. The model provides binding sites for both of the proton pump inhibitors, as exemplified by pantoprazole (Figure 4A) and the reversible K^+ competitive inhibitors such as SCH28080, Byk99, or Byk73 (Figure 4B,C). Although their mode of action is different, their inhibition is mutually exclusive, suggesting some overlap in their binding sites (*7*).

1,2α-Imidazopyridine Binding Sites. Inhibitor site modeling incorporated the disulfide-bound form of pantoprazole (Figure 4A) at Cys813 and Cys822 since these sites have been identified biochemically and the structure of the bound form is known (*33*). The disulfide bonds and the dimensions of the inhibitor provided constraints on the system during molecular dynamics and energy minimization. Favorable orientations within these constraints aligned the long axes of the inhibitors either between TM2 and TM9 helices in the case of Cys822 or along the TM5/TM6 extended loop when bound at Cys813 (Figure 2). Open sites adjacent to these residues therefore are predicted to have dimensions appropriate for the reversible inhibitor binding region. Strong evidence for the overlap in the sites for the two classes of inhibitor next to Cys813 is provided by the A335C mutant, which not only shows spontaneous cross-linking to Cys813 but is also the only mutant identified so far completely insensitive to SCH28080.

The region around Ala335 has been examined extensively by site-directed mutagenesis to define further the location of 1,2α-imidazopyridine binding. In these experiments mutant kinetic parameters, SCH28080 dissociation constant (K_i), apparent K_m, and V_{max}, are determined in ATPase assays, and mutations affecting K_i are identified. For the mutants presented here, specific activities could be characterized as barely measurable (Y340N), moderately inhibited (F315Y, R328E/Y324C, M330V, V331I, F332I, F333A, M334A, M334I, A335G, A335S, I336L, V338I, A339S,A339C, Y340F, L809C/F332C), insignificantly affected (V331F, F332C, F332Y, F333L, M334C, A335C, A335C/C813A, V337I, L809C), or apparently enhanced (G323E, F326W). Mutant $K_{m,app}$ values ranged from half to twice that of the wild type.

Several reported mutations (Table 1A, footnoted *b* and *c*) as well as various new mutations presented here change the K_i or the nature of the inhibition by SCH28080. These are consistent with the proposed binding region (Figure 5). Various mutations that have no effect on K_i (Table 1B) are also important for ruling out possible site locations. For instance, mutants G323E and F326W, substituted in the

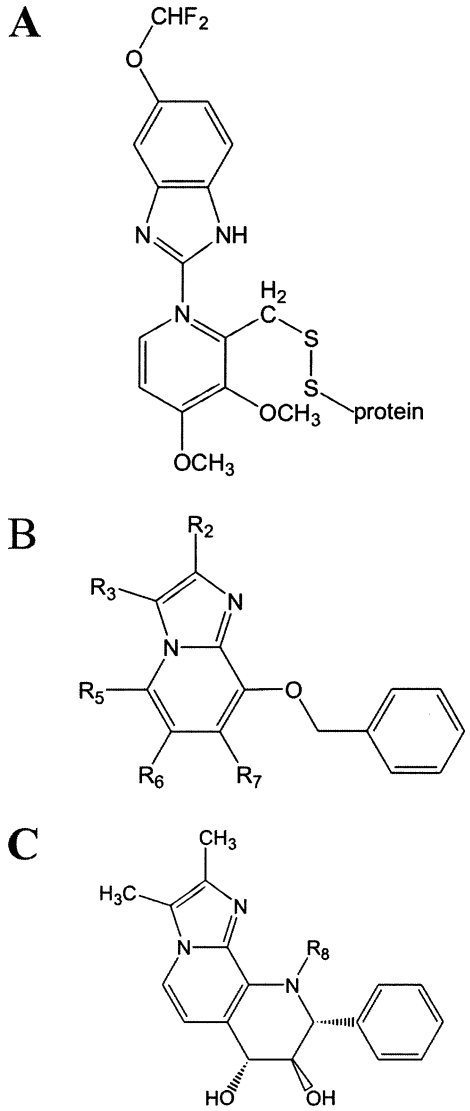

FIGURE 4: Inhibitors predicted to bind in the space next to the TM5/TM6 loop. (A) The protein-bound structure of the activated proton pump inhibitor, pantoprazole. (B) The core structure of SCH28080. (C) The K^+ competitive, bridged ring analogue of SCH28080 that has high affinity when R8 is H (Byk99) and low affinity when R8 is $-CH_3$ (Byk73). This effect is accounted for in the binding site model by unfavorable steric contact with the protein in the case of Byk73.

TM3/TM4 loop with the Na,K-ATPase residues, showed no effect on K_i, ruling out their side chains as binding site participants and suggesting a site deeper in the membrane domain. Similarly, the side chains of F333A or F333L, I336L, and V337I are on the opposite side of the TM4 helix from the proposed binding cleft, and these mutants show no effect on K_i. The side chain of V331F would be out of the site toward the lumen, and no effect is found for this mutant.

The most significant effects on the K_i were observed for mutants of Phe332, Ala335, and Leu809. In the case of the Phe332 mutants, only introduction of a β-branched side chain greatly decreased apparent affinity. Hence the steric requirement for binding is adjacent to the β carbon (Figure 5, F332 spheres). Accordingly, mutants F332C and F332Y show only 2- and 5-fold increases in K_i, respectively, while that of F332I (β-branched side chain) increased 62-fold compared to wild type. A similar effect was found for Met334 where the β-branched M334I (14-fold) gave greater loss of affinity than either M334C (8-fold) or M334A (7-fold). The β position of Met334 is predicted to be near the edge of the phenyl ring of the bound inhibitor (Figure 5, sphere).

In the case of Ala335, increasing side chain volume in the order G < A (wt) < S < C resulted in a progressive loss in affinity (K_i of 16, 64, and 1200 nM and no inhibition, respectively). The side chain of Ala335 faces directly into the middle of the imidazopyridine ring in the proposed binding site. There is apparently little tolerance for variations in the position of the inhibitor at this end since a compensatory increase in space at the other end of the cleft in the A335C/C813A double mutant did not regenerate significant inhibitor affinity (Table 1A). This novel series of mutations strongly supports the position occupied by these inhibitors in the membrane domain.

The previously reported mutants L809V and L809F showed a 5-fold and 96-fold loss of affinity (*23*). Leu809 is shown at the periphery of the site where only the L809F mutant is predicted to occupy a significant portion of the inhibitor binding space. The same authors reported 9-, 10-, and 5-fold increased K_i for P810G, L811F, and I816L while earlier work showed a 9-fold increase for C813T. These mutants further define the extent of the site in the vicinity of the TM5/TM6 loop and are consistent with the model of Figure 5.

Additional effects are given by ion site mutants K791S and E795D with ~20- and 11-fold reductions in SCH28080 affinity (*21*). It was not possible to bring the SCH28080 structure into close contact with these residues in the homology model. Glu795, however, makes hydrogen bond contact with Lys791 in the model and is the closest ion binding residue to the lumen. Alternative side chain dihedral angles can bring Glu795 within 5 Å of the imidazopyridine nitrogen of SCH28080 in the proposed bound form, possibly contributing to the charge environment of the inhibitor. It is also likely that distortion of the ion binding site has an allosteric effect on inhibitor binding. Evidence for a similar conclusion is that the E936D mutant in TM8 shows no change in the K_i but inhibition is strictly noncompetitive, clearly demonstrating separation of the two sites and a likely path for ion entry between TM8 and TM5. Other mutants changing the nature of inhibition to noncompetitive are L809F and L811F in the TM5/TM6 loop close to the proposed inhibitor site. These show large effects on the K_i and likely distort the bound conformation, allowing ion access to the transport site. A similar effect probably accounts for the mixed inhibition seen in many of the mutants.

The efficacy of a large number of compounds of the 1,2α-imidazopyridine class has provided structure/activity relationships for the ring positions, and this information is useful for excluding unacceptable binding modes (*5*, *6*). The availability of a large variety of these inhibitors is unique to the gastric H,K-ATPase. It has been shown that ring positions R1, R2, and R3 (Figure 4B) cannot be modified with groups larger than methyl (R1), ethyl (R2), or cyanomethyl (R3) without a dramatic loss in efficacy. Methyl group addition at R8 of Byk99 (Figure 4C) results in more than 1000-fold loss in binding affinity (data not shown). Larger substituents are permitted at R6 and, to a limited extent, at R5. In addition, the ring orientations in the enzyme-bound state have been defined for SCH28080 itself (*40*) by spectroscopic techniques and are consistent with the fixed ring positions

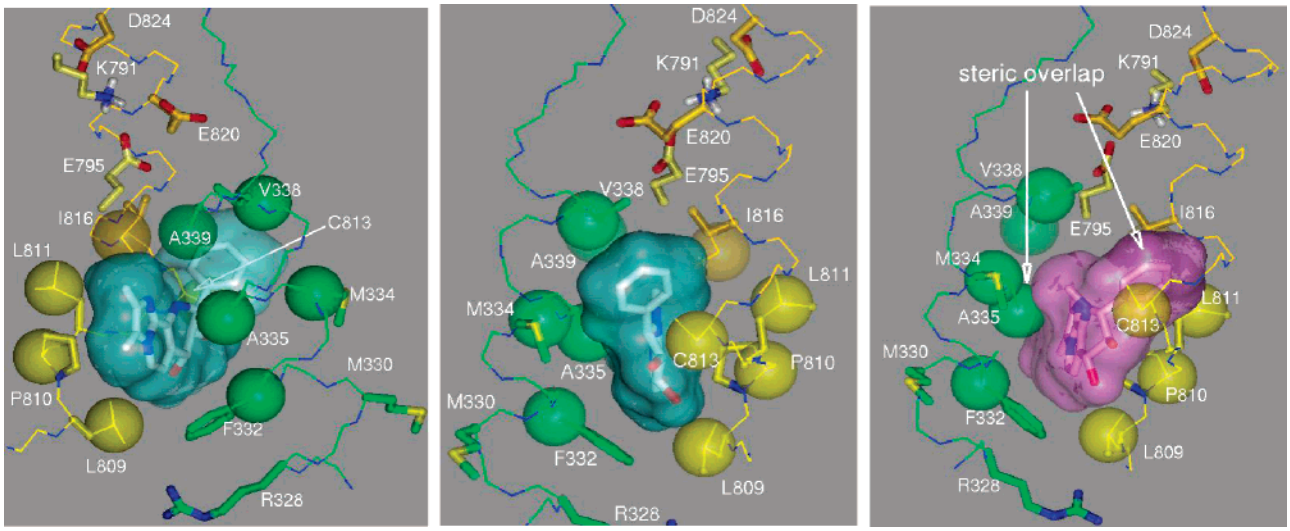

FIGURE 5: Views of the reversible inhibitor binding site from within the plane of the membrane as defined by effects of site-directed mutagenesis on K_i. Left: Bound Byk99 (stick form with Connolly surface in cloud) between TM4 (green), TM5/TM6 loop (yellow), and TM6 (gold) viewed from the same direction as in Figure 4. Center: View from the side opposite the left panel. Right: Steric overlap resulting from superimposing the imidazopyridine ring of Byk73, the methylated, low-affinity form of Byk99, onto the position of the imidazopyridine ring of bound Byk99. The site is partially enclosed by atom positions (spheres in CPK) where increased side chain volume affects inhibitor affinity (see Table 1A). The most significant decreases in K_i were given by A335C, F332I, M334I, and L809F. Hydrogens are omitted.

in the high-affinity derivative, Byk99, for which the stereochemistry is also known. The reversible binding mode described here for Byk99 (Figure 5) accounts for these observations.

SCH28080 may adopt a range of different conformations of equivalent energy upon rotation of the bonds between the imidazopyridine and phenyl rings. To eliminate these degrees of freedom, a binding orientation for the more rigid Byk99 was found in which the long axis of the imidazopyridine ring occupies the same cleft as pantoprazole at Cys813 with the para position of the phenyl moiety near Leu141 in TM2. Proximity to this part of the inhibitor is required, based on photoaffinity labeling of the TM1/TM2 region with a *p*-azido derivative of SCH28080 (*32*). Substituent size restrictions at R2 and R3 are accounted for by contact in these positions with the TM5 helix between Pro798 and Tyr799. In contrast, the permissive R5 and R6 positions face the open end of the cleft toward the lumen. Biochemical evidence suggests the binding form of the SCH28080 may be protonated (*6*), and the orientation shown brings the nucleophilic imidazo nitrogen into a position less than 8 Å below the carboxylate of Glu795. The space above this position is open, suggesting a path to the ion site. Finally, the set of side chains whose mutation decreased SCH28080 affinity defined the perimeter of the inhibitor site (spheres, Figure 5). The methylated form of Byk99, Byk73 (Figure 5, right, in pink), has much lower affinity than Byk99, and this is accounted for by its more kinked structure resulting in steric overlap with Cys813 and with the TM4 helix backbone at Ala335.

An alternative mode for SCH28080 binding to a homology model of the H,K-ATPase based on the E_2 conformation (database structure pbd.1kju) of the sr Ca-ATPase (*41*) was proposed previously (*42*) in which the plane of the imidazopyridine ring is approximately perpendicular to the axes of the membrane helices instead of in the vertical alignment proposed here. The horizontal arrangement was duplicated in a recent model (*43*). This mode was discarded here because the horizontally bound form could not account for the known structure/activity relationships of this class of inhibitor and, to the contrary, modification of permissive positions on the imidazopyridine ring resulted in extensive steric overlap with the protein. The current model accounts for these relationships as well as for the new set of mutation results especially in the region of the phenyl ring (Figure 5, center) and Ala335. In particular, the absence of inhibition in the A335C mutant was completely unexplained in the earlier, horizontal binding mode where Ala335 was not in direct contact with the bound inhibitor (*42*).

The current model proposes a significant separation between the luminal portion of TM4 and TM5/TM6, similar to that proposed for the exit conformation of the sr Ca-ATPase (*11*), and emphasizes the utility of the large number of K competitive inhibitors available for the H,K-ATPase as templates for this region of the enzyme.

Mechanism of Acid Transport. The stoichiometry of acid transport in gastric H,K-ATPase vesicles is known to be two protons (here assumed to be hydronium) in exchange for two luminal K^+ when measured at pH 6.1 in ion transporting gastric vesicles (*2*). The internal pH of these acid transporting vesicles is ~3.0. In vivo, however, the internal pH of the secretory canaliculus of the parietal cell is ~1.0, an acid gradient 3 orders of magnitude greater than in gastric vesicles, and the available free energy of ATP hydrolysis limits the stoichiometry to 1 H^+ for 1 K^+ per ATP in the catalytic cycle. We propose a possible mechanism for acid transport supported by mutagenesis of the carboxylic amino acids in the membrane domain (*21*) and various ion-bound forms of the H,K-ATPase E_2-P model. The carboxylates in the membrane domain (Glu343, Glu795, Glu820, Asp824, and Glu936) have been mutated previously to alternative carboxylate, amide, or aliphatic side chains. A carboxylate at position 820 is required for ion-stimulated activity (substitution with Asp active, Ala and Gln inactive) although very low K^+-independent ATPase activity has been described for E820Q (*44*). Hence, a negative charge in this position appears essential. In contrast, mutants E343Q, E795Q, and

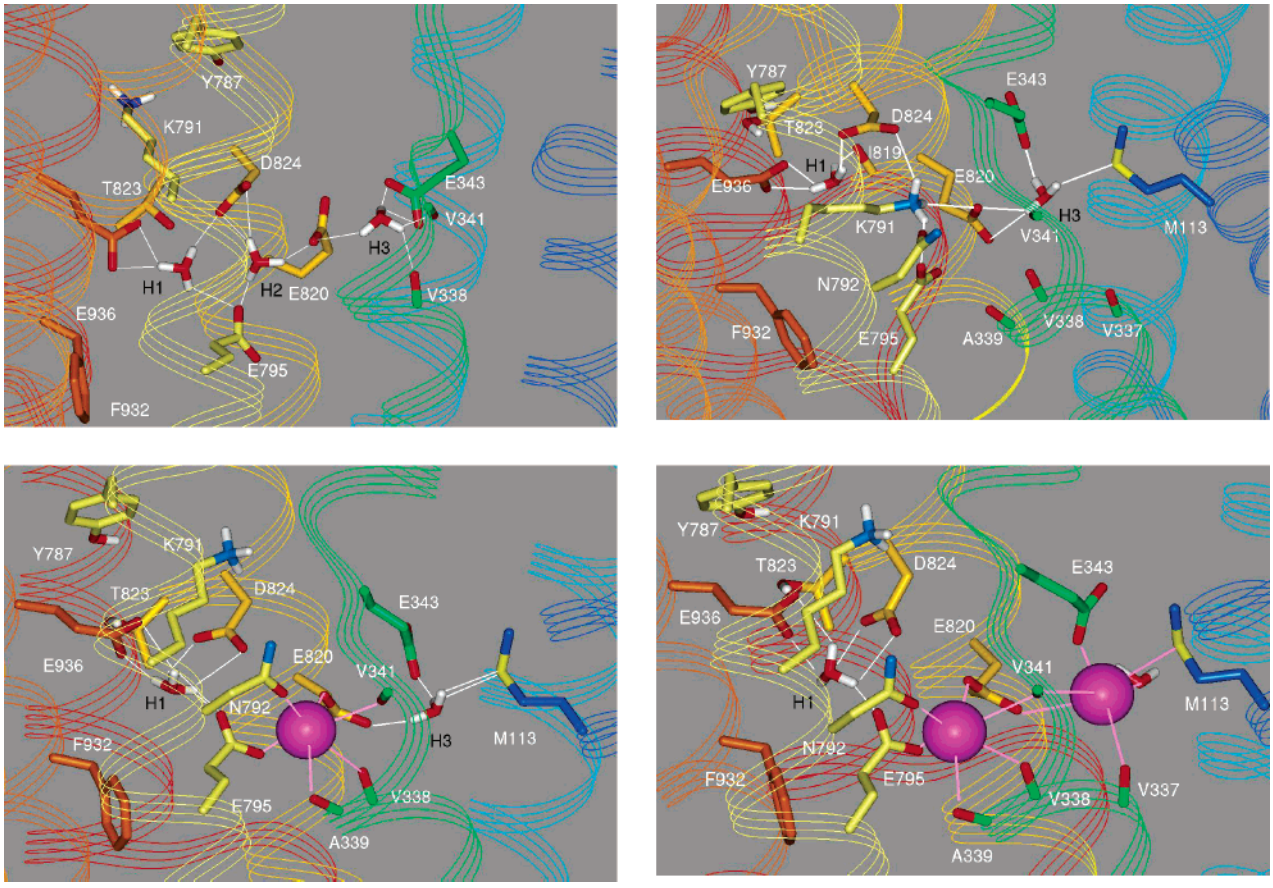

FIGURE 6: Hydronium release and K^+ binding to the H,K-ATPase E_1 and E_2P forms. Upper left: Hydronium site model (*21*) for the H,K-ATPase in $E_1 \cdot [3H_3O^+]$ based on the sr Ca-ATPase $E_1 \cdot [2Ca]$ structure, pdb.1eul (*9*). Hydroniums (at sites H1, H2, and H3) are placed between side chains homologous to those of the sr Ca^{2+} sites 1 and 2 and between these sites (H2). Hydrogen bonds (white lines) were maximized, and the model energy was minimized. Upper right: Ion site model for E_2-P with the amino group of Lys791 displacing hydronium from H2 in the acid transporting step to achieve a pK_a of ~1.0. Lower left: K^+ binding to E_2-P under acid transporting conditions displaces Lys791 to give the hypothetical model shown for $E_2 \cdot K^+$. Lower right: Theoretical ion site model for the H,K-ATPase in $E_2 \cdot 2K^+ \cdot K^+$ (purple spheres) are in 0.5 scale CPK. Ligand bonds are shown as purple lines. TM3 helix was omitted for clarity.

E936Q are active with 8%, 21%, and 22% of wild-type ATPase, respectively. Hydrogen-bonding capacity was shown to be essential at positions 343 and 936 where E343A and E936V were inactive. Side chain length was also important at position 343 with E343D showing no activity. Finally, K791 has a key role as shown by the activity measured for K791A and K791S mutants of 0% and 4% of wild type, respectively.

The transport site in the E_1 conformation must be able to load hydronium from the cytoplasm at neutral pH, well above the pK_a of a single, solvent-accessible carboxylate. This problem is apparently solved by clustering carboxylate side chains in the relatively hydrophobic environment of the ion site. This proximity effect is illustrated by the value of the second pK_a of fumaric acid (4.47) as compared to maleic acid (6.26). Here the dual effects of charge repulsion in the dianion and proton sharing between proximal carboxylates in maleic acid substantially decrease the dissociation constant for the second proton. These effects would apply in the H,K-ATPase. Specificity for hydronium in the ion site would arise from substitution of glutamate both at position 936 for the corresponding valine in the case of the Na,K-ATPase and also at position 820 for aspartate or asparagine in Na,K- and sr Ca-ATPases, respectively. These changes would increase the charge density of the site and bring carboxylate groups closer together compared to the other pumps.

A possible $E_1 \cdot [3H_3O^+]$ conformation for the H,K-ATPase is shown in Figure 5, upper left. Hydronium was fitted in a position analogous to Ca site 1, but the wider spacing of the transport site in the H,K-ATPase in E_1 (*21*) and increased length of Glu820 as compared to Asn796 of the sr Ca-ATPase resulted in greater distance to site 2. A single additional hydronium was insufficient to span both a site equivalent to Ca site 2 of sr Ca-ATPase and the Glu343 carboxylate although it seemed clear that the latter could not remain unprotonated in the presence of a luminal pH of 1. A minimal model thus appears to require three hydroniums which were arranged to optimize hydrogen bonding in forming sites H1, H2, and H3. Energy minimization then was performed to optimize the model shown. In this conformation Lys791 points toward the cytoplasm between TM6 and TM8.

In the E_2-P conformation there is a change in the relative positions of the TM5 and TM6 helices which brings Lys791 (Figure 6, upper left) more into the plane of the ion binding site (Figure 6, upper right). The orientation of the corresponding backbone position in the recently described E_2-P conformation of the sr Ca-ATPase (pdb.1wpg) is nearly identical (*11*). In this position, we propose the positively charged side chain amino group of Lys791 ($R-NH_3^+$) displaces hydronium from the H2 site in the acid transporting step. Charge pairing with Glu820 in the low dielectric of

the site would be essential in this step, as shown by the absolute requirement for a negative charge at position 820. Because of this charge compensation only the appropriate side chain length is necessary at position Glu795 to provide hydrogen bonding to Lys791 at the H2 site. Glu936 and Asp824 are closer together in E_2-P, forming a compact binding site for H_3O^+ which may in turn stabilize the Lys791 position by charge repulsion. Hence, inability to bind H_3O^+ efficiently in E936V, D824A, or D824N mutants would lead to severe impairment of function. The hydronium at the H3 site would remain at a luminal pH of 1.0.

The displacement of hydronium from site H2 by Lys791 as suggested here is consistent with the effects of mutating the homologous lysine (Lys800) in the toad bladder H,K-ATPase (*45*). This pump is also electroneutral and is known to transport Na^+ (*46*). However, a K^+-stimulated outward current was observed in Na^+-loaded oocytes injected with mutants K800A and K800E, showing that replacement of the positive charge resulted in Na^+ outward electrogenic transport. Conversely, the corresponding S782R mutant of the normally electrogenic toad Na,K-ATPase was electroneutral (*45*). In each case, charge mutation or replacement resulted in electrogenic behavior opposite to wild-type ATPase. A simple hypothesis would be that the positively charged side chain in the Na,K-ATPase mutant substitutes for one Na^+ in the forward step making the exchange two Na^+ for two K^+ and electroneutral. The toad bladder H,K-ATPase also transports Na^+, and replacement of the positively charged side chain at Lys800 would allow binding of the third Na^+ to give three Na^+ for two K^+ exchange to generate current. These data are consistent with the presence of the $R-NH_3^+$ group of Lys791 in the ion transport site and support its postulated role in the electroneutral mechanism of the gastric H,K-ATPase.

Another requirement of the mechanism is the ability to bind K^+ at low pH where entry from the lumen would first encounter Glu795 and Glu820 as potential ion ligands. Adjacent to these side chains is a nonhelical portion of TM4 which presents accessible carbonyl oxygens from Val338, Ala339, and Val341. These oxygens together with the side chain oxygen of Asn792 would be insensitive to protonation at pH 1. Appropriate octahedral geometry for K^+ binding was completed with oxygens from Glu820 and Glu795 whose optimal orientations are maintained in the model by hydrogen-bonding hydronium to their opposing oxygens (Figure 6, lower left). These hydroniums are in turn hydrogen bonded to Glu343 at H3 and Asp824 and Glu936 at H1. A recently published model of the H,K-ATPase has proposed a similar position for K^+ binding that included Asp824 and Glu343 as direct ligands (*47*) and is consistent with K^+ site 2 proposed for a homology model of the Na,K-ATPase (*48*). In the E_2-P model presented here these side chains are too far away to bind K^+ and must remain protonated (bind hydronium) at the low pH generated during acid transport in vivo. The charge state of the ion site side chains was not specified in the model of Koenderink et al. (*47*). The activity and high apparent ion affinity of the E795Q mutant is explained by the requirement for only one oxygen ligand contributed from this position and the low apparent ion affinity in E343Q by suboptimal hydronium bonding. Conversely, the apparent ion affinity of the E795D mutant was more than 3-fold lower than wild type, and this is explained by the shorter length of the side chain. Conversion to $E_1 \cdot K^+$ would be favored by the increased positive charge density next to Glu820 as previously suggested (*44*) and possibly by displacement of Lys791 to a position more similar to that assumed in E_1 (Figure 4, lower left).

At neutral pH, hydronium at the H3 site would dissociate because of a greater separation between Glu820 and Glu343 in E_2 compared to E_1. Replacement with luminal K^+ at this site would give the energy-minimized structure in Figure 6, lower right, and account for two H_3O^+ for two K^+ exchanged per ATP at the higher luminal pH ($\geq$3.0) found in vitro. Participation of Glu343 is supported by the finding that the mutant E343Q is active but has a 4-fold lower apparent ion affinity compared to wild type. An octahedral ligand set for this postulated site included a H_2O ligand, the sulfur atom of Met113, carboxylate oxygens from Glu343 and Glu820, and carbonyl oxygens of Val341 and Val337 (Figure 6). Although charge compensation for K^+ is mostly provided by Glu820, it appears ion-activated conversion to E_1 requires a contribution from position 343, providing either a hydrogen bond to H_3O^+ at the H3 site under acid conditions or an oxygen ligand for the second K^+ at neutral pH. This is because both E343A and E343D are inactive while E343Q has 8% wild-type activity.

In the Na,K-ATPase a site close to H1 has been proposed for K^+ binding (*48*) on the basis of the arrangement of available oxygen ligands and the finding that mutation of Ser782 lowered K^+ but not Na^+ affinity. The structure of a K^+ binding site in this position would have to be substantially different in the H,K-ATPase. Instead of an oxygen-bearing side chain, the H,K-ATPase substitutes positively charged Lys791 in place of Ser782, and this would appear to be destabilizing with respect to K^+ binding. The H,K-ATPase mutant K791S, however, shows 2-fold lower NH_4^+ affinity compared to wild type and is nearly inactive (*21*). Furthermore, the H,K-ATPase has Glu936 in H1 where the Na,K-ATPase apparently substitutes valine. Hence the site could compensate for the lack of serine by utilizing Glu936, and while the E936Q mutant has wild-type NH_4^+ affinity, that of E936D is decreased 2-fold. In the E_2-P model, however, there appeared to be insufficient ligands for an octahedral K^+ binding site next to the carboxylate of Glu936. Phe932 is one helix turn toward the lumen from Glu936 and was considered as a possible ligand, but the F932L mutant shows wild-type activity and ion affinity (*23*) indicating no involvement of the π electrons of the ring. The binding of K^+ at a site near H1 in the H,K-ATPase remains to be clearly demonstrated. Alternatively, we have suggested that hydronium remains bound at H1 between E936 and D824 during the catalytic cycle based on the small change in the relative positions of these side chains. Finally, the sr Ca-ATPase shares the a similar sequence with the H,K-ATPase in the cytoplasmic half of TM8 with Glu908 corresponding to Glu936 in the H,K-ATPase. Hydronium binding in the position equivalent to H1 in E_2-P is consistent with proton countertransport observed in the sr Ca-ATPase.

In summary, site-directed mutations and homology modeling of the membrane domain of the gastric H,K-ATPase have helped to define the three-dimensional position of both the covalent and K^+ competitive class of acid secretory inhibitors and have provided evidence for the mechanism of H^+ for K^+ exchange catalyzed by this enzyme. Further cysteine

cross-linking and mutagenesis approaches are being used currently to test the predicted orientation of TM1 and TM2 segments with respect to the other TM helices and the bound reversible inhibitors. During the preparation of this report, the structure of the sr Ca-ATPase crystallized with magnesium fluoride was published (*11*). This conformation, representing an E_2-P homologue, will provide valuable information for further refinement of the H,K-ATPase model. The major difference between this and previous structures of the sr Ca-ATPase is an increased separation of the luminal end of TM4 from the surrounding transmembrane segments, which is mimicked in our model by the constraints due to the site of K^+ competitive inhibitors and suggests homology to the luminal ion exit and entry conformations of the H,K-ATPase.

APPENDIX

Modeling of H,K-ATPase. Model building and energy minimizations were performed with Discover and InsightII molecular modeling software version 2000 (www.accelrys.com). The steps taken in the modeling were as follows:

(1) Amino acid sequences of the rabbit gastric H,K-ATPase α subunit and sr Ca-ATPase were aligned by using a combination of BLAST and manual adjustments (see Figure 7).

(2) The E_2·thapsigargin conformation (E_2[TG], pdb.1iwo) of the sr Ca-ATPase solved by X-ray crystallography provided the starting peptide backbone for the H,K-ATPase which was modeled from Glu49 to Ser1025.

(3) A modified backbone was built by deleting the backbone in pdb.1iwo where the aligned H,K-ATPase had gaps and re-forming peptide bonds from resulting free ends. H,K-ATPase sequence inserts required construction of loops which were derived from database structures giving the best overlap in their backbones with pdb.1iwo 3−7 residues on either side of the insert. An exception was a long insert in the P domain from T589 to D668 which was built de novo as a helix−loop−extended chain based on the predictive scheme of Rost et al. (*49*).

(4) In contrast to the M, A, and P domains where there are only a few short inserts/deletions between the sr Ca-ATPase and H,K-ATPases (except for that noted above in the P domain), the N (nucleotide binding) domain has several long sequence inserts and gaps. The Na,K-ATPase, however, has just a single proline deletion compared to the H,K-ATPase in the N domain. Therefore, the backbone atoms of the N domain of the α2 subunit of pig Na,K-ATPase, solved by X-ray crystallography (pdb.1q3i), were superimposed with a minimum RMS deviation onto pdb.1iwo according to the structural alignment described by Hakansson (*27*; see Figure 7). The backbone of the Na,K-ATPase N domain from Val381 to Ile585 then was inserted in place of the sr Ca-ATPase N domain (replacing the Val363 to Leu600; see Figure 10). It is important to note the structural alignment is completely unpredicted by sequence alignments using current algorithms (e.g., BLAST 2), and homology modeling based on pdb.1iwo alone would be inaccurate for the N domain. Certain disordered loops are unspecified in the pdb.1q3i file, and these were incorporated from the backbone structure (*50*) of the rat N domain solved by NMR techniques (pdb.1mo7). A single loop insertion for the extra proline in the N domain completed the H,K-ATPase backbone.

(5) The H,K-ATPase side chains 49−1025 were mapped onto the new backbone. All aspartates, glutamates, lysines, and arginines were added in their charged states. Obvious steric clashes were corrected manually. Side chain dihedral angles within one standard deviation of allowed mean values documented in high-resolution protein structures were used (*51*). The preferred side chain dihedrals in helices have been documented, and values within these ranges were used (*52*).

(6) Magnesium (+2 charge), inorganic phosphate, and three active site water molecules were added in the positions defined for the phosphoserine phosphatase (pdb.1j97) of *M. jannaschii* crystallized with the acyl phosphate analogue Mg-BeF_3 (*28*). This enzyme has a homologous active site fold to that of the P_2-type ATPases, and a similar position for the phosphate group in the sr Ca-ATPase has been described recently (*11*).

(7) The known bound structure of the proton pump inhibitor pantoprazole, an analogue of omeprazole, was then covalently linked via disulfide bonds to the side chain sulfurs at Cys813 and Cys822 where it is known to bind (*53*). SCH28080 binding prevents binding of omeprazole to the enzyme at Cys813 (*7*). All proton pump inhibitors bind to Cys813, and pantoprazole also binds to Cys822. Incorporation of the pantoprazole moiety binding at Cys813 therefore provides an effective volume and structural constraint for the inhibitor site vestibule in the E_2 conformation. Rotation of the disulfide dihedral angles revealed only one likely orientation for pantoprazole at Cys813, and this was along the groove between the TM5/TM6 loop and TM4. This provided a template for binding of the reversible inhibitors. The position of pantoprazole at Cys822 was less restricted, and it was assigned a starting position with its long axis roughly parallel to TM6 and between TM2 and TM9 helix axes.

(8) Distance restraints (range 2.9−3.1 Å, force constant 3 kcal/mol) were added to all helix donor/acceptor pairs. Additional restraints were applied to hydrogen bonds within the active site and to Mg/ligand distances (range 2.0−2.1 Å, force constant 3 kcal/mol) homologous to those in phosphoserine phosphatase (pdb.1j97). The most important of these involved side chains in the T[724]GDGVND loop which folds away from the active site in pdb.1iwo. The model then was energy minimized to an average absolute derivative less than 0.1 kcal (mol Å)$^{-1}$ with a medium dielectric constant of 15 and a nonbonded cutoff distance of 25 Å (used for all subsequent minimizations and molecular dynamics). Potentials, partial charges, and the force field [consistent valence force field (cvff)] were those supplied by the software manufacturer. Template forcing was applied during the minimization to bias the superimposition of homologous backbone segments on to the pdb.1iwo structure as suggested by sequence homology and defined for the N domain by Hakansson et al. (shown in bold in Figure 7). This procedure generated an initial model with homologous sequences in positions close to those of pdb.1iwo (RMS backbone deviation for the bolded sequences of Figure 7, 1.99 Å). The restrained structure was then submitted to a short molecular dynamics run at 300 K (1 fs time steps, 5.0 ps total with 0.1 ps of equilibration). At the end of the run the total energy was nearly constant, and the restrained distances in the active site, including those involving the T[724]GDGVND loop, had reached their final values

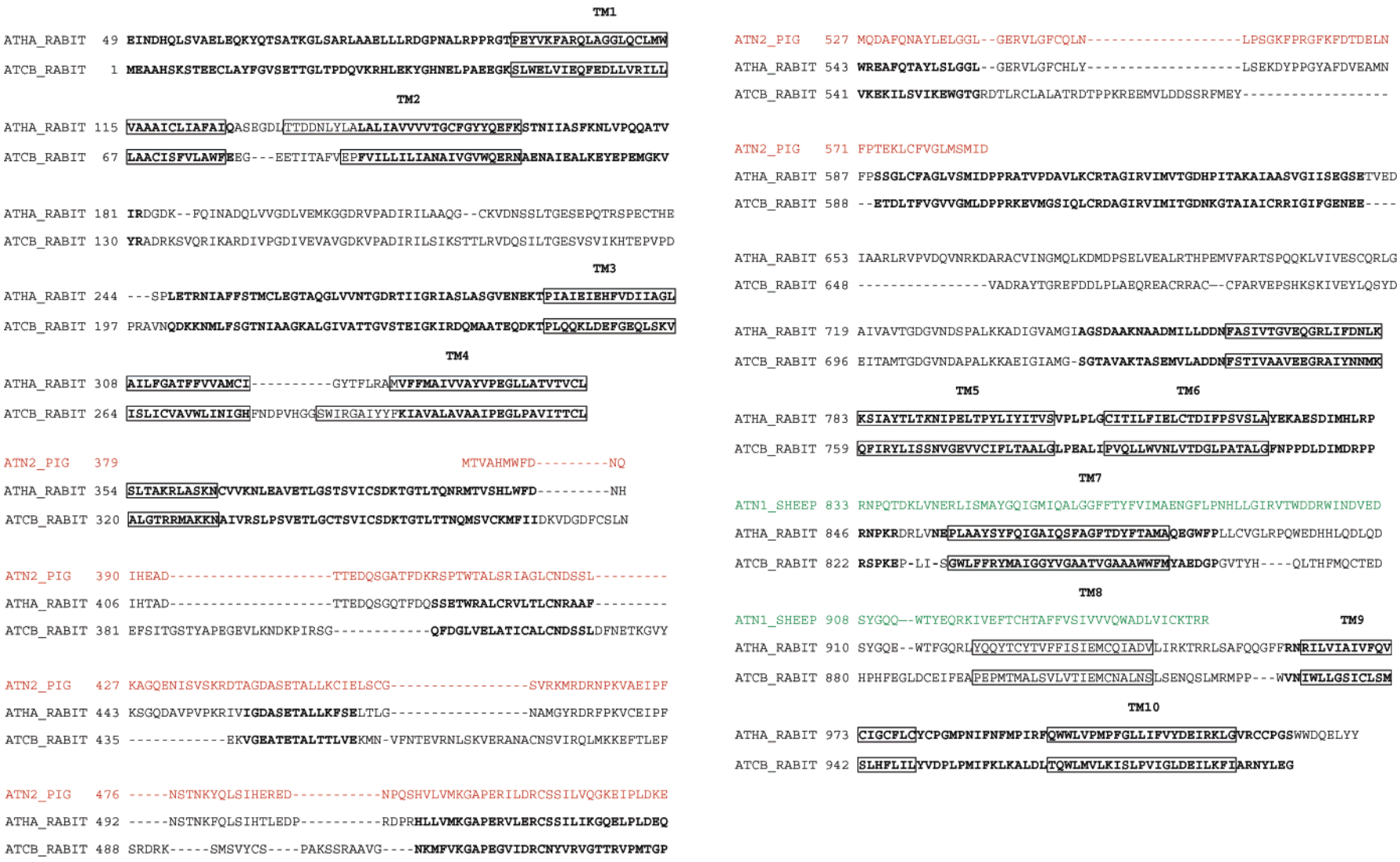

FIGURE 7: Sequence alignment of the rabbit H,K-ATPase α subunit (ATHA) and the rabbit sr Ca-ATPase (ATCB). This alignment was used for homology modeling. Boxed regions show the full length of sr Ca-ATPase helices that include the membrane domain segments and also extend into the stalk in TM2, TM4, and TM5. Helical structure (boxed) covers the same sequence segments in the homology model except where loop modeling required extending or truncating helices in TM2 and TM4, respectively, at their luminal ends. Sequences used for template forcing and calculation of the RMS deviation of superimposed backbone positions are in bold. The sequence alignment shown for the N domain of the pig Na,K-ATPase α2 subunit (ATN2) was determined by superimposing the three-dimensional structure onto the N domain of the sr Ca-ATPase (*27*). Alignment of the sheep Na,K-ATPase α1 sequence (green) in the TM7/TM8 loop through TM8 (green) illustrates the rationale for side chain assignments in this region. The lysine at position 791 in the H,K-ATPase is italicized.

(distances varied randomly around the mean with each time step).

(9) The structure given by molecular dynamics was then energy minimized with the restraints described above to an average absolute derivative less than 0.1 kcal (mol Å)$^{-1}$ to give the final pantoprazole-bound model. The RMS backbone deviation for the bolded sequences of Figure 7 was 2.83 Å. The RMS backbone deviation for matching segments in the N domain compared to the starting Na,K-ATPase template, pdb.1q3i, was 1.82 Å.

(10) The bound pantoprazoles were then removed, and the imidazopyridine ring of Byk99, a high-affinity, fixed-ring analogue of SCH28080 with known stereochemistry, was superimposed on the position occupied by the benzimidazole ring of pantoprazole at Cys813. This binding mode oriented the phenyl ring of Byk99 toward the TM1/TM2 helix pair as required by photoaffinity labeling found for a *p*-azido derivative of SCH28080 (*32*). Byk99 was used because the ring bridge removes rotational degrees of freedom accessible by SCH28080, giving the final minimized structure a higher probability of reproducing the true bound conformation. The bridge further constrains Byk99 in the active conformation known to interact with the inhibitor site (*40*). Molecular dynamics (300 K, 5.0 ps) and energy minimization were performed as described above to yield the final SCH28080 binding form with Byk99 in place of SCH28080.

(11) The model proposed for the $E_1{\cdot}3H_3O^+$ conformation utilized the previously reported E_1 structure of the H,K-ATPase membrane domain (*21*). Two hydronium ions (partial charges of 0.37 on the hydrogens and −0.11 on the oxygen) were added in positions equivalent to those shown for Ca^{2+} in the $E_1{\cdot}2Ca^{2+}$ form of the sr Ca-ATPase (pdb.1eul) and a third to a position between Asp824, Glu795, and Glu820. Minimization was performed without restraints to an average absolute derivative less than 0.1 kcal (mol Å)$^{-1}$.

(12) The ion site conformations proposed for $E_2{\cdot}K^+$ and $E_2{\cdot}2K^+$ utilized the final E_2-P model as a starting structure. Following removal of the inhibitor, K^+ was first placed between the side chains of Asn792, Glu795, and Glu820 and carbonyl oxygens of Val338, Ala339, and Val341 in a position similar to that proposed by Ogawa et al. for K^+ site 2 in a homology model of the Na,K-ATPase (*48*). This site appeared to have favorable geometry in the proposed acid transporting configuration of the ion site in E_2-P. For binding at neutral pH a second K^+ was given a starting position between Glu820, Glu343, and backbone carbonyl oxygens of Val341 and Val337 on the nonhelical portion of TM4 in a fashion similar to Ca^{2+} site 2 in the $E_1{\cdot}2Ca^{2+}$ form of the sr Ca-ATPase (pdb.1eul). This site further included a water molecule and also required the participation of the sulfur atom of Met113 to complete the octahedral ligand set. Energy minimization was performed as described above, including distance restraints in the range of 3.0−3.1 Å between the proposed ligands and K^+ in both $E_2{\cdot}K^+$ and $E_2{\cdot}2K^+$ models.

(13) The final models generated present a plausible explanation for the pK_a of one of the hydronium binding sites allowing secretion of 160 mM HCl as well as for the variable stoichiometry and for the binding sites and activities of both classes of inhibitors.

Sequence Alignments. There are a few important conclusions about the structure to be made from the sequence alignment used for homology modeling (Figure 7). First, the Na,K-ATPase does not appear to have an ion binding residue shared by the H,K-ATPase and the sr Ca-ATPases identified in TM8. This is illustrated by including a portion of the sheep Na,K-ATPase α1 sequence comprising TM7 to TM8 (green). In this region, the HK-ATPase has ISIEMCQ which matches VTIEMCN in the sr Ca-ATPase. The glutamate is a Ca^{2+} ligand in the $E_1{\cdot}2Ca^{2+}$ form of the sr Ca-ATPase (pdb.1eul). The H,K-ATPase also matches the Na,K-ATPase both before and after TM8, which results in the H,K sequence ISIEMCQ clearly aligning to VSIVVVQ of the Na,K-ATPase with no corresponding glutamate. Second, the alignment of the Na,K-ATPase α2 N domain (red) based on the crystal structure has not been predicted in previous alignments owing to the large loop differences. This advance greatly improved the probable accuracy of the model in this domain. Finally, the gaps inserted at the beginning of TM7 have not been included in previous alignments. The reasons for this adjustment are discussed above in the section describing the membrane domain.

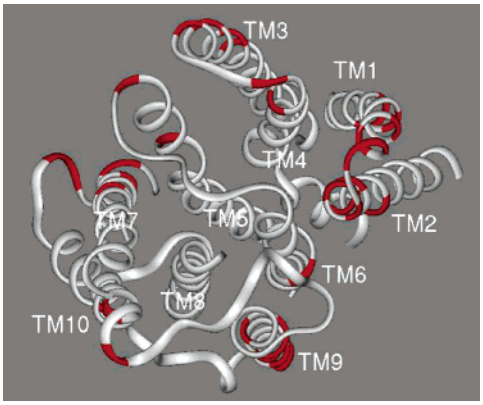

FIGURE 8: Ribbon display of the membrane domain of the H,K-ATPase E_2-P model viewed from the extracytoplasmic side showing the outward facing positions (red ribbon) of residue replacements in the highly homologous sting ray ATPase sequence. The large TM7/TM8 luminal loop is deleted for clarity.

Nonhomologous Replacements Face the Perimeter of the Membrane Domain. General support for the model in the membrane domain is illustrated by the positions of residue replacements found in the stingray α subunit (gb: AAP35241). This distantly related species shows remarkable homology to the rabbit (81% identity, 88% similarity using BLAST 2). Differences in the membrane domain consistently map to the noninteracting, outward facing surfaces of the TM helices or to the luminal loops as expected for a homologous protein (Figure 8). The absence of substitutions in the central region of the membrane domain (e.g., TM8) provides further evidence for a conserved arrangement of the TM helices among the sr Ca-ATPase and Na,K- and H,K-ATPases.

Active Site. Active site homology between the halo acid dehalogenase (HAD) proteins and the P-type ATPases noted previously (*54*) is confirmed in these crystal structures (e.g., pdb.1j97, pdb.1iwo). However, the sr Ca-ATPase in the E_2-[TG] conformation was crystallized in the absence of Mg^{2+} phosphate, and the -D[703]GVND- loop is too far from Asp351 to participate in Mg^{2+} phosphate binding in the manner seen for phosphoserine phosphatase. The active site of the E_2-P model of the H,K-ATPase was therefore energy minimized with restraints based on phosphoserine phosphatase, pdb.1j97, crystallized in the presence of Mg^{2+} and

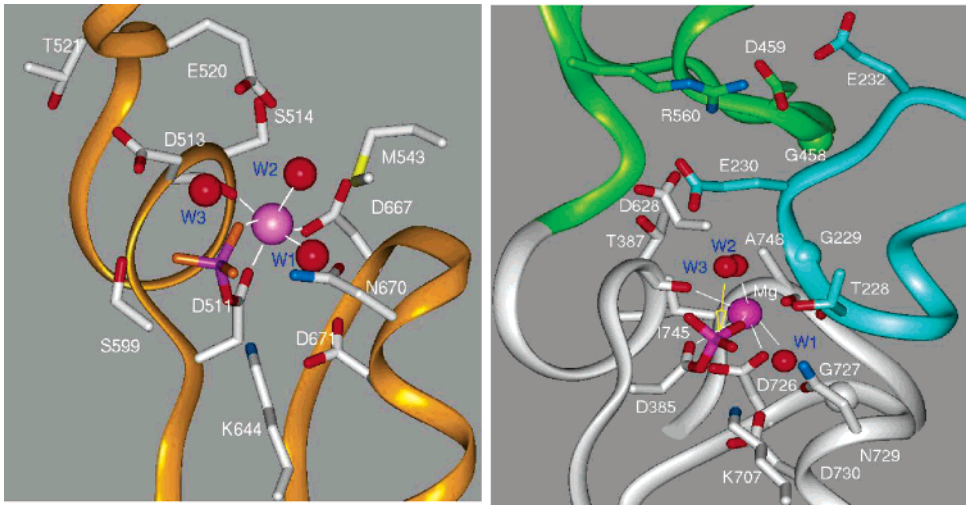

FIGURE 9: Active site structure. Active sites of phosphoserine phosphatase (pdb.1j97, left) and the H,K-ATPase E_2-P model (right) with side chains and phosphoryl group in stick form, waters (W1, W2, and W3), magnesium ion, glycine α carbons (spheres 0.5 scale CPK), and ligand bonds as white lines are shown.

BeF_3. Comparison of the phosphoserine phosphatase structure to the H,K-ATPase model illustrates the similarities and differences in the two enzymes (Figure 9).

Several available crystal forms of phosphoserine phosphatase (pdb 1f5s, 1j97, 1l7m, 1l7n, and 1l7p) were examined for conserved structure that could provide a basis for restraints in modeling the active site region of the H,K-ATPase in E_2-P. The most relevant of these for modeling the acyl phosphate form of the H,K-ATPase active site is pdb.1j97, which contains Mg^{2+} and BeF_3^{2-} as an acyl phosphate analogue. Common structures included a reverse turn containing the active site aspartate and a second loop opposing it with the consensus sequence DXXND (D[726]-GVND in the H,K-ATPase and D[667]GAND in PSP). Magnesium phosphate is bound between the two loops. A conserved lysine side chain (Lys644 in PSP and Lys707 in the H,K-ATPase) provides key hydrogen bonds to the active site aspartate, the phosphate, and the last aspartate in DXXND. The asparagine also supplies a hydrogen bond to phosphate which is further held in place by two hydrogen bonds to backbone amides on either side of the residue following the phosphorylated aspartic acid. Two waters bound to the magnesium ion are also found, one of which (W1 in Figure 9) is held in the DXXND loop by hydrogen bonds to both aspartates and the asparagine. In all of the structures the magnesium ligands include these two waters (W1 and W2 in Figure 9), a phosphate oxygen (or a fluoride), oxygens from the active site aspartate and the first aspartate in DXXND, and the backbone carbonyl oxygen of the second residue following the active site aspartate (Asp513 in PSP and Thr387 in the H,K-ATPase, Figure 9). Recently, all of these structural features have been observed in the E_2-P homologue of the sr Ca-ATPase (pdb.1wpg) crystallized in the presence of MgF_4^{2-}. In the phosphoserine structure pdb.1j97 a third water (W3 in Figure 9) is found in a nucleophilic position above the phosphate position, and this was included in the present model of the H,K-ATPase. Weak distance restraints were employed during energy minimization and molecular dynamics to mimic all of these conserved structural features in the E_2-P of the H,K-ATPase.

The resulting Mg^{2+} site in the E_2-P model (Figure 9, right) is somewhat larger than in phosphoserine phosphatase with ligand distances of 2.8 ± 0.05 Å. The interactions of W1 with Mg^{2+} and the D[726]GVND loop are nearly identical whereas those of W2 and W3 vary. W3 makes hydrogen bond contact with Asp513 in phosphoserine phosphatase. Glu230, W2, and the side chain of Thr626 (not shown) all appear within contact distance of W3 in the H,K-ATPase. The carbonyl oxygen of Thr387 is a Mg^{2+} ligand, making this a key residue. The position of W2 as a Mg^{2+} ligand in phosphoserine phosphatase is stabilized by interactions with Glu520 and Met543. In the H,K-ATPase model W2 is stabilized by hydrogen bonds to the phosphate and W3. The backbone oxygens of Ala746 (in the loop with inserted Ile745 as noted below) and Thr228 are 3.39 and 3.34 Å from the ion and therefore appear farther away than expected for direct ligands. Thr228 has been shown to play a role in vanadate binding and E_2-P stabilization (*55*).

The predicted arrangement of side chain ligands around the bound Mg^{2+} in the P domain is confirmed in the recently published structure (pdb.1wpg) of an E_2-P homologue of the sr Ca-ATPase (*11*). In that structure, however, the TGES loop is more displaced from the active site (farther forward from to perspective of Figure 9), and Thr181, equivalent to Thr228 of the H,K-ATPase, is too far away (6 Å) to be a Mg^{2+} ligand.

The loop positions around the active site Mg^{2+} of the model are supported by proximity to various sites of backbone cleavage given by treatment of the Na,K- and H,K-ATPases with ascorbate−H_2O_2−Fe^{2+} (*29*). These have been identified at Gly229 (A domain), Gly727 (P domain), and near Gly458 (N domain) with distances from Mg^{2+} (the site occupied by Fe^{2+} during the cleavage experiments) to the glycine α carbons (spheres, Figure 9) of 3.7, 5.7, and 9.1 Å, respectively. Hence the absence of a side chain to allow backbone accessibility may play a role in free radical cleavage efficiency. The cleavage site in the N domain is seen only in the presence of nucleotides and may originate from a second Fe site. In the E_2-P homologue of the sr Ca-ATPase (pdb.1wpg) the N domain has a different contact

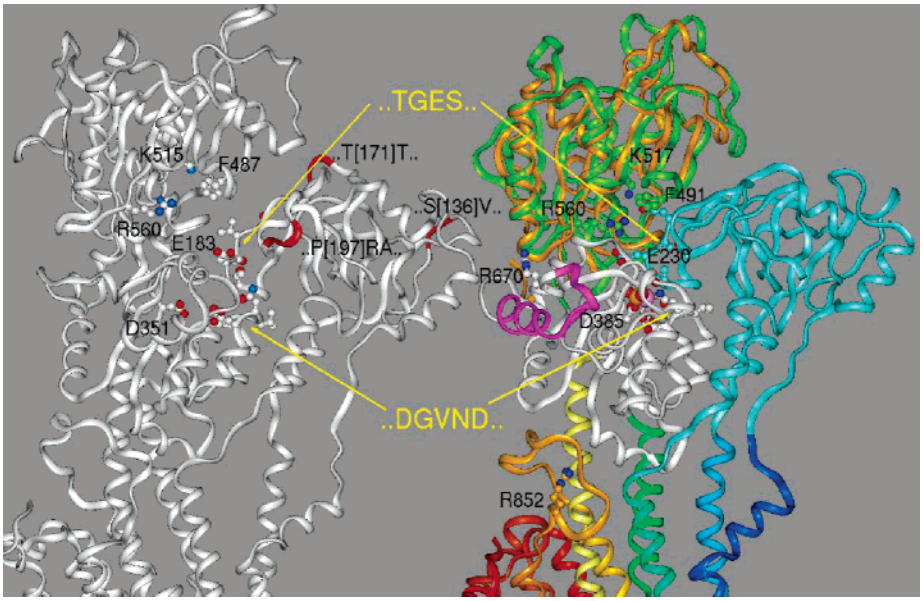

FIGURE 10: Comparison of the crystal structure of the cytoplasmic domain of the sr Ca-ATPase (left) in the E_2[TG] conformation and the H,K-ATPase E_2-P model structure (right) showing the change in position of two key loops (side chains in ball and stick representation), -D[726]GVND- in the P domain and -T[228]GES-in the A domain. The backbone of the Na,K-ATPase α2 N domain (gold ribbon) is superimposed on the corresponding H,K-ATPase N domain emphasizing the homology in this region. Short, surface-exposed loop deletions (red ribbon regions) in the A domain of the sr Ca-ATPase structure correspond to sequence deletions in the H,K-ATPase. A large loop insertion (purple ribbon) is present in the P domain of the H,K-ATPase. Trypsin cleaves the H,K-ATPase (*31*, *33*) at nonconserved, exposed positions in this loop (Arg670) and in a small loop just before TM7 (Arg852). The active site residues Asp351 of the sr Ca-ATPase and Asp385 of H,K-ATPase are shown in ball and stick representation. The adenine pocket lies between residues Lys571, Phe491, and Arg560 in the E_2-P model of the H,K-ATPase.

surface with the A domain than found for the H,K-ATPase model, and this results in a much greater distance (18.5 Å) from the active site to Gly438, the homologous residue to G458 of the H,K-ATPase. This gives greater accessibility to the adenine binding pocket than found in the model presented here. The E_2-P homologue of the sr Ca-ATPase, however, also contains MgADP bound in the nucleotide site, and this clearly affects the relative orientations of N and A domains as compared to E_2[TG].

Cytoplasmic Domain. The cytoplasmic domain of the H,K-ATPase model (Figure 10, right) shows subtle changes compared to the sr Ca-ATPase (pdb.1iwo, left). The N, P, and A domains are drawn together, making closer contact around the active site in the E_2-P form as detailed above. The upper half of the TM1 helix, above the bend point, is slightly raised, the TM2 helix moves into closer contact with TM4, and there is a slight forward rotation of the A domain as seen from the perspective of Figure 10.

The backbone of the H,K-ATPase N domain (green) closely superimposes (RMS 1.82 Å) the homologous Na,K-ATPase α2 N domain (pdb.1q3i in gold). The structure of the sr Ca-ATPase N domain is quite different as expected based on gaps and insertions in the sequence alignment (Figure 7). The overall shape of this domain in the H,K-ATPase is more elongated with extensive changes on the side opposite the interface with the A domain. A notable difference between the H,K- and sr Ca-ATPase is the loop beginning with Phe491 (in the N domain, just above the TGES sequence, Figure 10) which apparently extends farther out and makes more contact with the A domain in the H,K-ATPase than its counterpart in pdb.1iwo (Figure 10). The corresponding loop in the sr Ca-ATPase begins with Phe487 (ball and stick representation), a residue known to play a critical role in ATP binding. Despite the apparent loop differences, the respective positions of these phenylalanines next to the adenine binding cleft are very similar, suggesting homologous function (*9*).

A second critical residue in the N domain is Arg560 (ball and stick representation, Figure 10), which is known to have an important role in ATP binding. Experimental evidence supports interaction of the R560 side chain with oxygen of the β-phosphate (*16*), and this is confirmed in the E_1-[AMPPCP] structure of the sr Ca-ATPase (*9*). In the H,K-ATPase E_2-P model, Arg560 is centrally located between the carboxylates of Asp628, Glu230, Asp429, and Glu232. Arg560 would help to stabilize the arrangement of gathered cytoplasmic domains in E_2-P. In contrast, Arg560 makes no apparent hydrogen bonds in E_2[TG]. The Glu230 side chain occupies a position between the adenine binding pocket and the phosphorylation site (Figures 9 and 10). In this position Glu230 likely replaces the phosphate position upon dissociation of ADP as suggested for Glu183 in the sr Ca-ATPase (*12*).

The P domains show high homology except where the H,K-ATPase has a large insert, Thr649 to Asp668, modeled here as a helix−loop−extended chain based on the predictive scheme (*49*) of Rost et al. (purple ribbon). The position of the insert is well separated from the membrane and from the interacting A and P surfaces, making it a possible site of specific protein interaction or modification. The loop is solvent exposed near its C-terminal end as shown by selective trypsinolysis at Arg670 in the presence of SCH28080 and ATP (*32*). The structure associated with this loop is visible in Na,K-ATPase models resolved at 11 Å (*56*) or 9 Å (*57*). A second insertion of a single isoleucine (Ile745) is conserved in the H,K- and Na,K-ATPases and expands a loop close to the Mg^{2+} (pink sphere) in the active site. The functional significance of this insert is currently unexplored.

The A domain is also well conserved with just three short deletions (red ribbon segments) required in surface-exposed loops. These produce apparently minor changes (Figure 10). The conserved structure is indicative of strict control of function in the A domain. Proteinase K treatment of the sr Ca-ATPase cleaves a short segment leading to TM3 and results in normal phosphorylation from ATP to give $2CaE_1$-P but strongly impairs conversion to E_2-P (*58*) or even formation of E_2-P from P_i in the absence of Ca^{2+}. Hence one function of the A domain involves stabilization of E_2-P.

Mg^{2+} (pink sphere) at the active site and acyl phosphate bound to D385 (CPK) show the interface of the P and A domains. Close contact in the model between the -T[724]-GDGVND- loop and Mg^{2+} contrasts with pdb.1iwo, where this loop folds back and the active site is more open (Figure 10). Loop transfer to the active site during molecular dynamics and energy minimization was coupled to movement of the T[228]GES loop in the A domain. The two loops are in close contact in pdb.1iwo. These changes are associated with raising and rotating the A domain and with the T[228]-GES loop moving over the active site to give a more closed, solvent-inaccessible active site. A similar rotation of the A domain is seen in the E_2-P homologue of the sr Ca-ATPase (*11*). Exclusion of solvent is expected in E_2-P where hydrolysis of the acyl phosphate is under tight enzymatic control. In addition, the raised A domain results in closer contact between TM2 and the upper half of TM4. Together with the more compact N domain, these effects make the whole cytoplasmic domain of the H,K-ATPase model somewhat narrower than in pdb.1iwo.

In the sr Ca-ATPase, Arg560 participates in ATP binding via charge pairing with the β-phosphate in E_1·ATP, and the A domain is rotated away from the active site (*9*). The H,K-ATPase E_2-P model suggests that dissociation of ADP and conversion of E_1-P to E_2-P is associated with movement of the A domain to bring the loop containing Glu230 and Glu232 into the space over the active site and possibly into proximity with Arg560. A similar mechanism was proposed earlier on the basis of both Fe^{2+}-catalyzed cleavage in Na,K- and H,K-ATPases (*29*) and the crystallized structures of different conformations of the sr Ca-ATPase (*12*).

ACKNOWLEDGMENT

We are grateful to J. Senn-Bilfinger for his generous gift of Byk99 and Byk73.

REFERENCES

1. Polvani, C., Sachs, G., and Blostein, R. (1989) Sodium ions as substitutes for protons in the gastric H,K-ATPase, *J. Biol. Chem. 264*, 17854−17859.
2. Rabon, E. C., McFall, T. L., and Sachs G. (1982) The gastric [H,K]-ATPase:H+/ATP stoichiometry, *J. Biol. Chem. 257*, 6296−6299.
3. Besancon, M., Simon, A., Sachs, G., and Shin, J. M. (1997) Sites of reaction of the gastric H,K-ATPase with extracytoplasmic thiol reagents, *J. Biol. Chem. 272*, 22438−22446.
4. Kaminski, J. J., Bristol, J. A., Puchalski, C., Lovey, R. G., Elliott, A. J., Guzik, H., Solomon, D. M., Conn, D. J., Domalski, M. S., and Wong, S. C. (1985) Antiulcer agents. 1. Gastric antisecretory and cytoprotective properties of substituted imidazo[1,2-a]pyridines, *J. Med. Chem. 28*, 876−892.
5. Kaminski, J. J., Wallmark, B., Briving, C., and Andersson, B. M. (1991) Antiulcer agents. 5. Inhibition of gastric H+/K(+)-ATPase by substituted imidazo[1,2-a]pyridines and related analogues and its implication in modeling the high affinity potassium ion binding site of the gastric proton pump enzyme, *J. Med. Chem. 34*, 533−541.
6. Wallmark, B., Briving, C., Fryklund, J., Munson, K., Jackson, R., Mendlein, J., Rabon, E., and Sachs, G. (1987) Inhibition of gastric H+,K+-ATPase and acid secretion by SCH 28080, a substituted pyridyl(1,2a)imidazole, *J. Biol. Chem. 262*, 2077−2084.
7. Hersey, S. J., Steiner, L., Mendlein, J., Rabon, E., and Sachs, G. (1988) SCH28080 prevents omeprazole inhibition of the gastric H+/K+-ATPase, *Biochim. Biophys. Acta 956*, 49−57.
8. Toyoshima, C., Nakasako, M., Nomura, H., and Ogawa, H. (2000) Crystal structure of the calcium pump of sarcoplasmic reticulum at 2.6 Å resolution, *Nature 405*, 647−655.
9. Toyoshima, C., and Mizutani, T. (2004) Crystal structure of the calcium pump with a bound ATP analogue, *Nature 430*, 529−535.
10. Toyoshima, C., and Nomura, H. (2002) Structural changes in the calcium pump accompanying the dissociation of calcium, *Nature 418*, 605−611.
11. Toyoshima, C., Nomura, H., and Tsuda, T. (2004) Lumenal gating mechanism revealed in calcium pump crystal structures with phosphate analogues, *Nature* (in press).
12. Toyoshima, C., and Inesi, G. (2004) Structural basis of ion pumping by Ca2+-ATPase of the sarcoplasmic reticulum, *Annu. Rev. Biochem. 73*, 269−292.
13. Paula, S., and Ball, W. J., Jr. (2004) Molecular determinants of thapsigargin binding by SERCA Ca2+-ATPase: a computational docking study, *Proteins 56*, 595−606.
14. Toyoshima, C., Asahi, M., Sugita, Y., Khanna, R., Tsuda, T., and MacLennan, D. H. (2003) Modeling of the inhibitory interaction of phospholamban with the Ca2+ ATPase, *Proc. Natl. Acad. Sci. U S A. 100*, 467−72.
15. Asahi, M., Sugita, Y., Kurzydlowski, K., De Leon, S., Tada, M., Toyoshima, C., and MacLennan, D. H. (2003) Sarcolipin regulates sarco(endo)plasmic reticulum Ca2+-ATPase (SERCA) by binding to transmembrane helices alone or in association with phospholamban, *Proc. Natl. Acad. Sci. U S A. 100*, 5040−5045.
16. Jorgensen, P. L., Hakansson, K. O., and Karlish, S. J. (2003) Structure and mechanism of Na,K-ATPase: functional sites and their interactions, *Annu. Rev. Physiol. 65*, 817−849.
17. Sweadner, K. J., and Donnet, C. (2001) Structural similarities of Na,K-ATPase and SERCA, the Ca(2+)-ATPase of the sarcoplasmic reticulum, *Biochem. J. 356*, 685−704.
18. Arguello, J. M., and Lingrel, J. B. (1995) Substitutions of serine 775 in the alpha subunit of the Na,K-ATPase selectively disrupt K+ high affinity activation without affecting Na+ interaction, *J. Biol. Chem. 270*, 22764−22771.
19. Blostein, R., Wilczynska, A., Karlish, S. J., Arguello, J. M., and Lingrel JB. (1997) Evidence that Ser775 in the alpha subunit of the Na,K-ATPase is a residue in the cation binding pocket, *J. Biol. Chem. 272*, 24987−24993.
20. Peluffo, R. D., Arguello, J. M., and Berlin, J. R. (2000) The role of Na,K-ATPase alpha subunit serine 775 and glutamate 779 in determining the extracellular K+ and membrane potential-dependent properties of the Na,K-pump, *J. Gen. Physiol. 116*, 47−59.
21. Vagin, O., Munson, K., Lambrecht, N., Karlish, S. J., and Sachs, G. (2001) Mutational analysis of the K+-competitive inhibitor site of gastric H,K-ATPase, *Biochemistry 40*, 7480−7490.
22. Munson, K. B., Lambrecht, N., and Sachs, G. (2000) Effects of mutations in M4 of the gastric H+,K+-ATPase on inhibition kinetics of SCH28080, *Biochemistry 39*, 2997−3004.
23. Vagin, O., Denevich, S., Munson, K., and Sachs, G. (2002) SCH28080, a K+-competitive inhibitor of the gastric H,K-ATPase, binds near the M5-6 luminal loop, preventing K+ access to the ion binding domain, *Biochemistry 41*, 12755−12762.
24. Asano, S., Matsuda, S., Hoshina, S., Sakamoto, S., and Takeguchi, N. (1999) A chimeric gastric H+,K+-ATPase inhibitable with both ouabain and SCH 28080, *J. Biol. Chem. 274*, 6848−6854.
25. Farley, R. A., Schreiber, S., Wang, S. G., and Scheiner-Bobis G. (2001) A hybrid between Na+,K+-ATPase and H+,K+-ATPase is sensitive to palytoxin, ouabain, and SCH 28080, *J. Biol. Chem. 276*, 2608−2615.
26. Hersey, S. J., Steiner, L., Mendlein, J., Rabon, E., and Sachs G. (1988) SCH28080 prevents omeprazole inhibition of the gastric H+/K+-ATPase, *Biochim. Biophys. Acta 956*, 49−57.
27. Hakansson, K. O. (2003) The crystallographic structure of Na,K-ATPase N-domain at 2.6 Å resolution, *J. Mol. Biol. 332*, 1175−1182.

28. Cho, H., Wang, W., Kim, R., Yokota, H., Damo, S., Kim, S. H., Wemmer, D., Kustu, S., and Yan, D. (2001) BeF(3)(−) acts as a phosphate analog in proteins phosphorylated on aspartate: structure of a BeF(3)(−) complex with phosphoserine phosphatase, *Proc. Natl. Acad. Sci. U.S.A. 98*, 8525−8530.
29. Karlish, S. J. (2003) Investigating the energy transduction mechanism of P-type ATPases with Fe2+-catalyzed oxidative cleavage, *Ann. N.Y. Acad. Sci. 986*, 39−49.
30. Shin, J. M., Goldshleger, R., Munson, K. B., Sachs, G., and Karlish, S. J. (2001) Selective Fe2+-catalyzed oxidative cleavage of gastric H+,K+-ATPase: implications for the energy transduction mechanism of P-type cation pumps, *J. Biol. Chem. 276*, 48440−48450.
31. Besancon, M., Simon, A., Sachs, G., and Shin, J. M. (1997) Sites of reaction of the gastric H,K-ATPase with extracytoplasmic thiol reagents, *J. Biol. Chem. 272*, 22438−22446.
32. Munson, K. B., Gutierrez, C., Balaji, V. N., Ramnarayan, K., and Sachs, G. (1991) Identification of an extracytoplasmic region of H+,K(+)-ATPase labeled by a K(+)-competitive photoaffinity inhibitor, *J. Biol. Chem. 266*, 18976−18988.
33. Shin, J. M., Cho, Y. M., and Sachs, G. (2004) Chemistry of covalent inhibition of the gastric (H+,K+)-ATPase by proton pump inhibitors, *J. Am. Chem. Soc. 126*, 7800−7811.
34. Shin, J. M., and Sachs, G. (2004) Differences in binding properties of two proton pump inhibitors on the gastric H+,K+-ATPase in vivo, *Biochem. Pharmacol. 68*, 2117−2127.
35. Toyoshima, C., Asahi, M., Sugita, Y., Khanna, R., Tsuda, T., and MacLennan, D. H. (2003) Modeling of the inhibitory interaction of phospholamban with the Ca2+ ATPase, *Proc. Natl. Acad. Sci. U.S.A. 100*, 467−472.
36. Melle-Milovanovic, D., Milovanovic, M., Nagpal, S., Sachs, G., and Shin J. M. (1998) Regions of association between the alpha and the beta subunit of the gastric H,K-ATPase, *J. Biol. Chem. 273*, 11075−11081.
37. Colonna, T. E., Huynh, L., and Fambrough, D. M. (1997) Subunit interactions in the Na,K-ATPase explored with the yeast two-hybrid system, *J. Biol. Chem. 272*, 12366−12372.
38. Sachs, G., Shin, J. M., Besancon, M., and Prinz, C. (1993) The continuing development of gastric acid pump inhibitors, *Aliment. Pharmacol. Ther. 7* (Suppl. 1), 4−12 (discussion 29−31).
39. Richardson, J. S. (1981) The anatomy and taxonomy of protein structure, *Adv. Protein Chem. 34*, 167−339.
40. Watts, J. A., Watts, A., and Middleton, D. A. (2001) A model of reversible inhibitors in the gastric H+/K+-ATPase binding site determined by rotational echo double resonance NMR, *J. Biol. Chem. 276*, 43197−43204.
41. Xu C., Rice, W. J., He, W., and Stokes, D. L. (2002) A structural model for the catalytic cycle of Ca(2+)-ATPase, *J. Mol. Biol. 316*, 201−211.
42. Munson, K., Vagin, O., Sachs, G., and Karlish, S. (2003) Molecular modeling of SCH28080 binding to the gastric H,K-ATPase and MgATP interactions with SERCA- and Na,K-ATPases, *Ann. N.Y. Acad. Sci. 986*, 106−110.
43. Asano, S., Yoshida, A., Yashiro, H., Kobayashi, Y., Morisato, A., Ogawa, H., Takeguchi, N., and Morii, M. (2004) The cavity structure for docking the K(+)-competitive inhibitors in the gastric proton pump, *J. Biol. Chem. 279*, 13968−13975.
44. Swarts, H. G., Koenderink, J. B., Hermsen, H. P., Willems, P. H., and De Pont, J. J. (2001) K(+)-independent gastric H(+),K(+)-ATPase activity. Dissociation of K(+)-independent dephosphorylation and preference for the E1 conformation by combined mutagenesis of transmembrane glutamate residues, *J. Biol. Chem. 276*, 36909−36916.
45. Burnay, M., Crambert, G., Kharoubi-Hess, S., Geering, K., and Horisberger, J. D. (2003) Electrogenicity of Na,K- and H,K-ATPase activity and presence of a positively charged amino acid in the fifth transmembrane segment, *J. Biol. Chem. 278*, 19237−19244.
46. Grishin, A. V., and Caplan, M. J. (1998) ATP1AL1, a member of the non-gastric H,K-ATPase family, functions as a sodium pump, *J. Biol. Chem. 273*, 27772−27778.
47. Koenderink, J. B., Swarts, H. G., Willems, P. H., Krieger, E., and De Pont, J. J. (2004) A conformation-specific interhelical salt bridge in the K+ binding site of gastric H,K-ATPase, *J. Biol. Chem. 279*, 16417−16424.
48. Ogawa, H., and Toyoshima, C. (2002) Homology modeling of the cation binding sites of Na+K+-ATPase, *Proc. Natl. Acad. Sci. U.S.A. 99*, 15977−15982.
49. Rost, B., and Sander, C. (1993) Secondary structure prediction of all-helical proteins in two states, *Protein Eng. 6*, 831−836.
50. Hilge, M., Siegal, G., Vuister, G. W., Guntert, P., Gloor, S. M., and Abrahams, J. P. (2003) ATP-induced conformational changes of the nucleotide-binding domain of Na,K-ATPase, *Nat. Struct. Biol. 10*, 468−474.
51. Ponder, J. W., and Richards, F. M. (1987) Tertiary templates for proteins. Use of packing criteria in the enumeration of allowed sequences for different structural classes, *J. Mol. Biol. 193*, 775−791.
52. Richardson, J. S., and Richardson, D. C. (1989) Principles and Patterns of Protein Conformation, in *Prediction of Protein Structure and the Principles of Protein Conformation* (Fasman, G. D., Ed.) pp 1−99, Plenum Press, New York.
53. Sachs, G., Shin, J. M., Vagin, O., Munson, K., Weeks, D., Scott, D. R., and Voland, P. (2002) Current trends in the treatment of upper gastrointestinal disease, *Best Pract. Res. Clin. Gastroenterol. 16*, 835−849. Review.
54. Stokes, D. L., and Green, N. M. (2000) Modeling a dehalogenase fold into the 8-Å density map for Ca(2+)-ATPase defines a new domain structure, *Biophys. J. 78*, 1765−1776.
55. Toustrup-Jensen, M., and Vilsen, B. (2003) Importance of conserved Thr214 in domain A of the Na+,K+-ATPase for stabilization of the phosphoryl transition state complex in E2P dephosphorylation, *J. Biol. Chem. 278*, 11402−11410.
56. Rice, W. J., Young, H. S., Martin, D. W., Sachs, J. R., and Stokes, D. L. (2001) Structure of Na+,K+-ATPase at 11-Å resolution: comparison with Ca2+-ATPase in E1 and E2 states, *Biophys. J. 80*, 2187−2197.
57. Hebert, H., Purhonen, P., Vorum, H., Thomsen, K., and Maunsbach, A. B. (2001) Three-dimensional structure of renal Na,K-ATPase from cryo-electron microscopy of two-dimensional crystals, *J. Mol. Biol. 314*, 479−494.
58. Moller, J. V., Lenoir, G., Marchand, C., Montigny, C., le Maire, M., Toyoshima, C., Juul, B. S., and Champeil, P. (2002) Calcium transport by sarcoplasmic reticulum Ca(2+)-ATPase. Role of the A domain and its C-terminal link with the transmembrane region, *J. Biol. Chem. 277*, 38647−38659.

BI047761P